Review

THE CHEMICAL RECORD

doi.org/10.1002/tcr.202400266
tcr.wiley-vch.de

Advances in Electrocatalyzed Water Oxidation by Molecular Complexes of First Row Transition Metals

Chiara Lenzi,[a, b] Andrea Masetti,[a, b] Isacco Gualandi,[a, b] Erika Scavetta,[a, b] Luca Rigamonti,[c] and Rita Mazzoni*[a, b]

Abstract: Energy transition toward sustainable, alternative, and affordable solutions is likely to be one of the major challenges of the anthropocene era. The oxygen evolution reaction (OER) is a pivotal electrocatalytic process essential for advancing renewable energy conversion and storage technologies, including water splitting, artificial photosynthesis, metal-air batteries, and fuel cells. Electrocatalytic pathways can significantly reduce the overall energy requirements of these devices, particularly focusing on the energy demands associated with water splitting for hydrogen production. This review, after introducing the state of the art in heterogeneous catalysis, will be devoted to the description of molecular water oxidation electrocatalysts (MWOCs), focusing on the recent advancements on catalysts composed of various metals, including Mn, Co, Cu, Ni, and Fe, in combination with a range of mono- and multidentate ligands. Critical insights are presented and discussed to provide readers with suggestions for ligand design in assisted catalysis. These observations aim to identify synergistic solutions that could enhance technological maturity by reducing energy absorption while improving stability and efficiency.

Keywords: Electrocatalysis, homogeneous catalysis, earth abundant, oxygen evolution reaction, hydrogen

1. Introduction

The growing climate concerns, alongside the rapid rise in global energy demands, require an acceleration in the energy transition toward the development of sustainable, alternative, and affordable energy solutions. In this context, artificial photosynthesis, able to capture solar energy in chemical bonds to be lately used as solar fuel, has attracted considerable attention as a promising approach to address these critical societal challenges.[1] This objective has been approached by photocatalytic and electrocatalytic pathways, looking forward promising strategies that harness visible light as the primary energy source to drive water splitting reactions, offering practical solutions for a clean and sustainable hydrogen fuel economy.[2]

Notably, sunlight-driven water splitting, which involves two half-reactions that split water into molecular hydrogen and oxygen, encounters a key limitation in the oxidation of water to O_2, i.e. in the oxygen evolution reaction (OER), due to the kinetic and thermodynamic cost of this half reaction.[3] Therefore, one of the main challenges to become competitive with this strategy lies in discovering water oxidation catalysts (WOCs) that are highly efficient, selective, and stable.

Due to the large demand of water splitting technologies, the cost reduction of catalysts is expected to be one of the driving forces of new strategies and processes. Low-cost catalysts, focusing on advancements from the perspective of heterogeneous (inorganic) materials, primarily feature: low

[a] *C. Lenzi, A. Masetti, I. Gualandi, E. Scavetta, R. Mazzoni*
Department of Industrial Chemistry "Toso Montanari", via Gobetti, 85, 40129 Bologna, Italy
E-mail: rita.mazzoni@unibo.it
[b] *C. Lenzi, A. Masetti, I. Gualandi, E. Scavetta, R. Mazzoni*
Center for Chemical Catalysis – C3, University of Bologna, via Gobetti, 85, 40129 Bologna, Italy
[c] *L. Rigamonti*
Department of Chemical and Geological Sciences, University of Modena and Reggio Emilia, via G. Campi 103, 41125 Modena, Italy

loading noble metal catalysts, active materials containing earth-abundant transition metal, carbon- based and hybrid catalysts.[4] To minimize the use of precious metals, further advancements in the rational design of electronic structures and topology are required to enhance both activity and stability.[5] Alloys, oxides, and composites based on Ir and Ru represent the bases for the most active and stable catalytic species for OER. Although the activity trends ($Ru > Ir \approx RuO_2 > IrO_2$) still favour metals and alloys, the reactivity trend toward dissolution ($Ru \gg Ir > RuO_2 \gg IrO_2$) highlights the oxides as more promising in both the acidic and basic medium. However, further investigations are needed to ensure suitable stability for large applications.[6]

Large interest has also been directed toward the low cost and good corrosion resistance of earth-abundant transition metal oxides.[7] Indeed, their multivalent oxidation states make them excellent candidates for OER. Chemical composition, crystallographic structure, pore structure morphology of the

Rita Mazzoni received her Ph.D in Chemistry in 2005 from the University of Bologna. Currently she holds a position as Associate Professor in Inorganic Chemistry at the Department of Industrial Chemistry (University of Bologna). Her main research interests are focused on the rational design of homogeneous catalytic systems for sustainable biomass conversion (e.g. bio-oil mixtures, HFM and bio-ethanol valorization) and energy transition (water oxidation, hydrogen production, acqueous phase reforming) based on noble and Earth-abundant transition metal complexes.

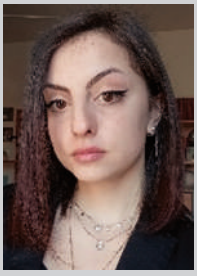

Chiara Lenzi received her Bachelor of Science in Industrial Chemistry in 2021 and her Master of Science in Industrial Chemistry in 2023, both from Alma Mater Studiorum – University of Bologna, Italy. She is currently a PhD student under the supervision of Prof. Rita Mazzoni at the University of Bologna, focusing on the synthesis, characterization, and study of organometallic complexes for biomass valorization, including scale-up processes. Since 2024, she has been a research fellow working on homogeneous catalysis. Her research background includes studies on N-heterocyclic carbene-based catalysts for water oxidation and noble metal nanoparticles for wastewater treatment

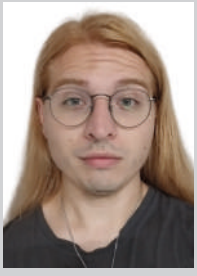

Andrea Masetti obtained his M.Sc. in Low Carbon Technologies and Sustainable Chemistry from the University of Bologna in 2021. Following a year of research under a grant, he began his Ph.D. in Industrial Chemistry under the supervision of Prof. Rita Mazzoni. His research focuses on the development and synthesis of novel, low-cost, and sustainable metal chelates for agricultural applications. These innovative fertilizers aim to enhance soil fertility in nutrient-deficient regions, contributing to more sustainable and efficient farming practices

Luca Rigamonti is associate professor of General and Inorganic Chemistry at the Università degli Studi di Modena e Reggio Emilia, Italy. He awarded his PhD in Chemical Sciences at the Università degli Studi di Milano in 2007. He moved to Modena as a Postdoc in 2011, where he became tenure track researcher in 2018 and then associate professor in 2021. His research activity is focused on the synthesis, spectroscopic and structural characterizations of coordination and organometallic molecular systems, and the study of their reactivity and magnetic, optical, catalytic and biological properties upon modulation of their electronic and steric features.

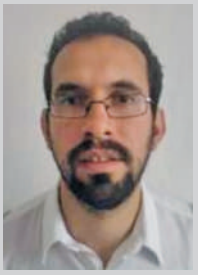

Isacco Gualandi graduated in Industrial Chemistry summa cum laude in 2009 and he accomplished his PhD studies in Chemical Sciences in 2013 at the Bologna University. After a period of post-doctoral fellowships at the Departments of physics and and Industrial Chemistry, he worked as a researcher at UNIBO. He is now an associate professor in analytical chemistry, and his research activity focuses on the development of innovative electrochemical sensors based on both inorganic and organic materials.

oxygen binding surface, and electronic structure of individual active sites are among the parameters that influence activity. As an example, cationic (e.g., Ni, Fe, Co, Mn, Sn) and anionic (e.g., O, S, OH) regulation has been proven to be a well-being method to tune the electronic structure improving the activity.[4b,8] Mixed-metal oxides, like Ni/Co(O),[9] Ni/Fe-(O,)[10] Li/Co(O),[11] allowing porous and complex structures, are also stable and efficient due to favorable contact area between the electrolyte and reactants. On the other hand, hydroxides (e.g. based on Mn, Fe, Co and Ni with different morphology), mainly structured as layered hydroxide[12] with a cationic brucite-like layers separated by interlayer anions, exhibit promising electrocatalytic activity. This performance is largely attributed to their open structure, with $Ni(OH)_2$[13] standing out as the most effective among single hydroxides. Moreover, binary[14] and ternary[15] hydroxides exhibit enhanced activity toward OER. Thanks to their flexibility in structures and compositions, perovskites with general structures ABO_x (with A: alkaline or rare earth metal, B: transition metal) allow a large variability that is revealed to be useful for OER with crystal vacancies playing a significant role in the construction of active catalysts. Interestingly $Ba_{0.5}Sr_{0.5}Co_{0.8}Fe_{0.2}O_3$ reached higher OER activity compared to IrO_2 in alkaline medium.[16] Higher stability than oxide is ensured also by transition metal (Ni, Co, Mn) phosphates/phosphides.[17] Finally, carbon-based materials, known for their excellent stability, high conductivity, and large surface area (e.g. carbon nanotubes (CNTs), graphene, nanocarbons and mesoporous carbons) are highly appealing in the OER field. Their geometrical and electrical structure can be further tuned by doping with third, fifth or sixth group elements in the electrode material decreasing the activation energy for the process while also enhancing the activity up to overtaking IrO_2.[18]

The importance of tuning the shape and structure of electrocatalytic materials has driven researchers toward more intricate domain of hybrid nanostructures, such as carbon based-, graphene based-, nitride based- materials and more, obtaining high carrier mobility and long-term durability.[19] A must have, for high performance, is a strong bond between the catalyst materials and the working electrode. As interesting examples, hybrid cobalt–hydroxide nanowires coated with graphitic carbon nitride[20] nanosheets allowed better capabilities than $Co(OH)_2$, IrO_2, RuO_2, and g-C_3N_4 with a low overpotential of 320 mV at 10 mA cm^{-2} for water oxidation; core-branch hydroxysulfides like $Co_2NiS_{2.4}(OH)_{1.2}$ also exhibited peculiar OER performance (overpotential 279 mV at 10.0 mA cm^{-2}), a low Tafel slope (52 mV dec^{-1}), [*vide infra for definition*] and a good long-term stability.[21]

As extensively known, Nature employs intricate sunlight driven biochemical systems for water oxidation to O_2. The critical step of O – O bond formation is coupled to the release of two protons, O_2 generation and rapid release, followed by a water-binding event. All these simultaneous processes are assisted by proper metals in well-defined oxidation states, by hydrogen bonding networks controlled by aminoacid residues. Simultaneously, electrons and protons derived from water are employed to drive the reduction of CO_2.[22]

With the goal of duplicating this fascinating and complicated process, the synergistic interaction between metals and their ligand environment can be more precisely tuned in molecular complexes. This is why homogeneous, heterogenized and hybrid catalytic systems are receiving increasing attention due to their higher efficiency, atom economy, well defined active sites and tunability, although stability often remains their Achille's heel.[23]

In this review the recent advances in design, characterization and mechanistic insight on molecular catalysts for OER (Molecular Water Oxidation Catalysts – MWOC) will be presented and discussed. Starting from a comparative discussion on the characterization employed in heterogeneous vs. homogeneous cases, the review will cover the most recent developments approaching earth abundant metal complexes. The huge amount of literature concerning noble metal complexes, such as Ru based MWOCs, extensively described in several review documents[24,25] will be briefly summarized to have countability of the gap to be covered to reach applicability with first row MWOCs. Then, manganese, cobalt, copper, nickel and iron complexes[25,4b,c] with particular accent to recent developments, design and results, will be critically described to complete the current picture of the state of the art in the field, and suggest new directions for the unsolved problem such as instability and kinetic challenges.

2. Assessment of OER Electrocatalysts Performance

OER occurs at the electrode surface and involves a series of proton-electron coupled processes that convert water into molecular oxygen.[26] The efficiency and mechanism of OER are significantly influenced by the pH and electrolyte of the reaction medium.[26a] In acidic and neutral environments, two water molecules are oxidized to produce one molecule of oxygen and four protons. Conversely, in basic conditions, hydroxyl ions are oxidized, resulting in the formation of water and oxygen.

The processes involved in OER, along with their equilibrium half-cell potentials, are summarized below:

In an acid aqueous electrolyte

$$2H_2O \rightarrow O_2 \uparrow + 4H^+ + 4e^- \quad E = +1.229\,V$$

In basic aqueous electrolyte

$$4OH^- \rightarrow O_2 \uparrow + 2H_2O + 4e^- \; E = +0.401\,V$$

Since reaction kinetics are a crucial aspect of oxygen evolution, significant overpotentials are necessary to achieve high rates of water-to-oxygen conversion.[3d] Therefore, the use of electrocatalysts or electrode materials with high activity is crucial for minimizing the energy consumption of electrochemical devices that rely on this reaction. Heterogeneous metal oxide catalysts have been employed in water electrolysis for many years and serve as the industrial benchmark.[3d] As a result, much of the literature has focused on evaluating the performance of heterogeneous electrodes for the OER.[27] When characterizing homogeneous electrocatalysts, it is important to consider the key parameters that define heterogeneous catalysts to ensure meaningful comparisons with mainstream literature. The most important parameters are overpotential at defined current density, Tafel slope, turnover frequency (TOF), faradaic efficiency (FE) and stability.[3b,26a, 27] Before assessing the electrocatalytic performance, it is essential to characterize the electrocatalyst film from a physicochemical perspective. Key factors to consider include chemical composition, crystallographic structure, morphology, thickness, conductivity, material quantity in the film, as well as its electrochemical properties. Equally important, due to the heterogeneous nature of the OER process, are the wettability and aerability of the film.

The electrocatalytic process should be validated through control experiments that compare the behavior of electrodes modified with active materials to that of bare electrodes. The OER should occur at lower potential values on the modified electrode than on the bare electrode. Typically, the OER wave overlaps with the redox processes underlying electrocatalysis. Therefore, it is not possible to carry out an independent electrochemical characterization of the redox couple of the catalyst facilitating this process, as one might in ideal electrocatalytic scenarios. Although significant research efforts have been made to study the chemical and morphological structure of OER catalysts during operation using hyphenated techniques[28,29,30] such as X-ray diffraction, X-ray absorption, Raman spectroscopy, and mass spectrometry (including ESI-MS),[31] electrochemical characterization must be primarily devoted to identifying specific potential values associated with the redox process. The onset potential refers to the potential at which the electrocatalytic process induces a sharp increase in current.[32] Although many papers report values for the onset potential, a universally accepted definition is not readily available. To achieve a more rigorous evaluation of the characteristic potential at which the electrocatalytic process occurs, the literature often assesses the overpotential measured when a specific current density is reached. Commonly used current density values are 10 and 100 $mA\,cm^{-2}$, but commercial devices typically require current densities that exceed at least 500 $mA\,cm^{-2}$.[4a] This value is usually expressed in relation to the thermodynamic potential observed for oxygen evolution in the specific medium.

The Tafel slope and exchange current density are important parameters that provide valuable insights into the activity of catalysts, reaction kinetics, and OER mechanisms. The Tafel equation indicates that the logarithm of the current is linearly related to the potential. The slope of the linear portion of this curve is known as the Tafel slope, which represents the potential change required to increase the electrocatalytic current by one order of magnitude. A low Tafel slope value indicates high electrocatalytic performance.[33] Another parameter that can be derived from this analysis is the exchange current density, which is determined by evaluating the current that would flow when the overpotential is zero. A high exchange current density indicates good catalytic activity.[32] The kinetics of the reaction can also be assessed using the TOF, which is ideally defined as the number of O_2 molecules produced per active metal site per second. TOF is calculated from the current density at a specified potential and the number of active sites on the electrode.[34] Overall electrochemical processes can be influenced by various phenomena, such as diffusion, solution resistance, mass transport, and charge transfer, which are not strictly related to chemical kinetics. FE is defined as the ratio of the amount of O_2 produced (as measured by an independent analytical method) to the theoretical amount of O_2 produced based on the charge that flows at the electrode. It is crucial to assess the selectivity of the OER in the specific reaction medium.

All the kinetic parameters discussed can be correlated with the mass or volume of the electrocatalyst employed. A crucial factor in evaluating catalyst performance for the OER is stability under operating conditions. This is especially important because the OER can generate highly oxidizing species that may degrade or cause the solubilization of the materials comprising the electrocatalysts. Stability is assessed through experiments that monitor the behavior of overpotential (or current) while a constant current density (or potential) is applied.[12]

The study of homogeneous electrocatalyst performance should be carefully planned, taking into account the technological maturity of the compounds being investigated. Characterization procedures developed for heterogeneous systems can be readily adapted for use in aqueous environments. Control experiments are essential for effectively demonstrating the electrocatalytic properties of these materials. The potential formation of heterogeneous active materials on the electrode surface is a crucial factor to consider during the characterization of homogeneous electrocatalysts.[3b] Acquiring voltammograms at various scan rates and in electrolytes with differing pH levels can yield valuable insights that further support the

electrocatalytic properties of the materials under examination.[35]

In the early stages of study, demonstrating the electrocatalytic properties in the OER reaction plays a key role and can also occur in solvents other than water. In this case, the redox couple responsible for the electrocatalysis can be easily studied in the absence of OER, allowing for a characterization that is closer to that of a traditional electrocatalytic system. The addition of H_2O or aqueous solutions to the reaction environment leads to an increase in the peak current of the anodic wave and a decrease in the peak cathodic current, as expected for a traditional electrocatalytic process.[36] The characterization of these systems usually involves identifying kinetic parameters such as the catalytic constant and TOF, through specific procedures for homogeneous catalysts.[37]

3. Ruthenium MWOCs: A Brief Overview

As mentioned above, there is already a considerable number of reviews concerning noble metal complexes, especially ruthenium-based MWOCs.[24,25] Nevertheless, even if the focus of the present review is first row transition metal MWOCs, it is mandatory to give a brief overview of noble metal molecular species able to act as valuable catalysts. This indeed can help discuss the advances with Earth abundant metals and their efficiencies.

Ruthenium systems have been studied since 1982 mainly with dinuclear complexes[38] and then moved to most active mononuclear species,[39] and they absolutely dominate the OER field because of their high stability and adaptability with consequent extraordinary turnover frequencies.[40] Furthermore, ligands can stabilize various oxidation states from II to V through changes in their geometrical and electronical features,[41] a key point to carry out the demanding $4e^-/4H^+$ water oxidation.

Neutral nitrogen-donor heterocyclic systems first appeared as promising ligands for mononuclear ruthenium complexes,[24b] followed by their functionalization with carboxylate, sulphonate or phosphonate moieties reaching outstanding TONs and lower catalytic potentials compared to neutral counterparts,[42] either electrocatalytic or employing sacrificial oxidants. $[Ru^{II}(tda/bda)(L)_2]$-type complexes (H_2tda = [2,2′:6′,2″-terpyridine]-6,6″-dicarboxylic acid, H_2bda = [2,2′-bipyridine]-6,6′-dicarboxylic acid, ancillary ligands L = pyridine, picoline, etc.) possess sufficient flexibility on the ligand side to allow intramolecular proton transfer with concomitant low activation energy. Furthermore, proton-coupled oxidation behavior is observed, with pK_a around 3–4 for $[Ru^{III}–OH_2]^+$ intermediates, which start the catalytic cycle and evolves into hydroxido ruthenium(IV) and oxido ruthenium(V) species.[43] The substitution of carboxylate moieties with phosphonate and sulfonate groups in the bda scaffold is supposed to act as proton relays either in the first or second coordination sphere, enabling the proper orientation for reactivity. Other secondary sphere modifications, such as pendant nitrogen bases, also make an important contribution. TONs can exceed 1,000,000 in some cases,[44] Electrocatalytic TOFs goes up to 16,000 s^{-1} at neutral pH when phosphonates are present,[45] and overpotential are usually between 400 and 600 mV, but also with examples as low as about 130 mV by inserting isoquinoline-based ligands.[46]

Catalytic $[Ru^{II}(tda/bda)(L)_2]$-type species have been also engineered to form oligomeric assemblies through the use of bridging ditopic ligands like 4–4'-bipyridine, ready to be adsorbed over supports like multiwalled carbon nanotubes due to their aromatic terpyridyl or bipyridyl scaffold,[47] but they can also be anchored into triazine-based frameworks functionalized with pyridyl tails able to coordinate ruthenium[48] or incorporated into iron-based metal-organic frameworks (MOFs) for the realization of integrated devices for artificial photosynthesis.[49]

An interesting advancement is also given by ruthenium complexes with redox-active polypyridyl ligands that can be electronically modulated by inserting electron donating or withdrawing substituents on their scaffold. This class of ruthenium MWOCs displays water oxidation reactivity with Ru(IV) = (O) intermediates at reasonable rates and with low overpotentials between 110 and 300 mV depending on the substituent.[50]

Finally, Ru complexes provide valuable insights into the potential mechanisms of O–O bond formation.[51] These mechanisms for Ru complexes can be broadly categorized into two pathways: 1) the water nucleophilic attack (WNA) pathway, in which a water molecule attacks an oxygen atom of high-valent metal–oxo species, and 2) the radical coupling (RC) pathway, which involves the coupling of two metal–oxo units possessing radical character.

4. First Row Complexes for Electrochemical Water Oxidation

4.1. Manganese Complexes for Electrocatalytic Water Oxidation

As outlined in the introduction, manganese-based WOCs have drawn extensive attention due to their ability to mimic the oxygen-evolving complex (OEC) in photosystem II (PSII), a critical system in natural photosynthesis. It consists of a Mn_4CaO_5 cubane cluster that facilitates the four-electron oxidation of water to molecular oxygen with exceptional efficiency and high TOF (100–400 s^{-1}) and serve as a blueprint for synthetic WOCs, enabling mechanistic insights and structural inspiration.[25a] Research on manganese based molecular electrocatalysts range from 1983 to date. Recent

developments have focused on the design of mononuclear or multinuclear complexes, which have proven to be the most promising.

Mn_4CaO_5 Cubane Analogues: Synthetic efforts to replicate the Mn_4CaO_5 cluster have included heterometallic cubane compounds. For example, Zhang et al.[52] synthesized a biomimetic Mn_4CaO_4 cluster with a dangling Mn ion. The inclusion of calcium proved critical for bio-assembly, solvent interactions, and catalytic activity. Replacing Ca^{2+} with heavy metals like Gd^{3+} modulated ligand basicity, offering strategies for constructing multinuclear analogs. These studies elucidated spectroscopic and magnetic properties across different S-states preceding O–O bond formation.

Manganese Adamantane Structures: Tetranuclear manganese adamantane complexes, such as those developed by Wieghardt et al.,[53] featured $[Mn^{IV}_4O_6]^{4+}$ aggregates coordinated with 1,4,7-triazacyclononane ligands. Armstrong and others[54] synthesized variants using tridentate amine and iminodicarboxylate ligands, broadening the understanding of ligand influences on reactivity.

Phosphine-Based Cubane Complexes: Dismukes[55] reported μ-oxo bridged $Mn^{III}_2Mn^{IV}_2$ cubane complexes with phosphine ligands, showcasing unique structural characteristics and catalytic properties.

Nonplanar Butterfly Complexes: Vincent et al.[56] developed non-planar butterfly-type complexes ($[Mn_4(\mu_3\text{-}O)_2(\mu\text{-}O_2CR)_7(bpy)_2]^{n+}$), capable of $Mn^{II}_2Mn^{III}_2$ to Mn^{III}_4 oxidations. These systems displayed diverse redox behavior, emphasizing the impact of coordination geometry.

Heterometallic Mn-Ca Complexes: Agapie's[57] group studied Mn_3Ca cubane models, emphasizing calcium's role in achieving high oxidation states. Variants incorporating heavy metals (Gd^{3+}) or silver ions revealed modulation effects on ligand properties: inclusion of these ions modulate the basicity of the coordinating μ-oxo ligands and exerts a rational strategy for the construction of multinuclear OEC analogues.

Binuclear Manganese Systems: Naruta et al.[58] explored bio-inspired manganese triphenylporphyrin (TPP) systems linked via phenylene-amidic bridges, both in mono or dinuclear metal center system, where the metal center can be easily oxidized to high valence state. This group also reported TPP complexes via o-phenylene bridges, achieving significant reactivity (TON 9.2) despite higher oxidation potential. Mechanistic studies confirmed oxygen evolution from solvent water using mass spectrometry and isotope labeling. Similar complexes bearing ligands containing xanthene and corrole by Akermark et al,[59] allowed a more rapid oxygen generation from the addition of Bu_4NOH. Both gave rise anyway to small amounts of molecular oxygen. Other multidentate N/O ligands by Styring and co-workers[60] were reported in a systematic screening of the ability of dinuclear manganese complexes to serve as MWOCs, with a different mechanism suggested by full incorporation of labeled water. Finally, a more recent dinuclear manganese terpyridine-based complex was employed as a catalytic precursor in an aqueous medium by Raj and Padhi in 2022.[61] Nevertheless, at pH 6.0, redox responses led to the electrodeposition of heterogeneous species, identified as MnO_x, which facilitated the oxidation process as confirmed by not diffusion control and XPS analysis. The oxidation process occurred at an applied potential of 0.99 V versus SCE, resulting in the release of 50.2 μmol/L of O_2 with FE of 97%. This example underline the importance to be aware of the final destination of the molecular catalyst to understand the real active species.

Mn-Oxo Clusters: Christou[62] reported a fascinating Mn_{12}-oxo cluster $[Mn_{12}O_{12}(O_2CC_6H_3(OH)_2)_{16}(H_2O)_4]$ (Mn_{12}DH), highly soluble and stable in water. Prepared from cheap and environmentally friendly precursors, it well performs as a stable homogeneous water oxidation electrocatalysts with an interestingly low overpotential (334 mV) under slightly acidic conditions (pH = 6). This behavior highlights the influence of multinuclear arrangements on catalytic efficiency.

Mononuclear Manganese Systems: Li et al.[63] described a multidentate mononuclear Mn-based systems (Figure 1 – **Mn 1**) capable of electrochemical water oxidation to O_2 at pH 12.2 applying 1.23 V in aqueous solution with TON of 20. The most recent mononuclear Mn complex active as electrocatalyst in water oxidation is from J. Lin group.[64] They reported on a water soluble, stable clathrochelate complex with the formula of $[Mn^{IV}(L\text{-}_6H)]^{2-}$ (Figure 1- **Mn 2**), that showed a high stability, an onset overpotential of 540 mV and a TOF of 0.3 s^{-1} working in phosphate buffer solution at pH 8.0.

This work usefully underlines the critical importance of the multidentate hydrazide ligand for the stabilization of higher oxidation states on the Mn center, which forms as active intermediates during the catalytic reaction.

4.2. Cobalt Complexes for Electrocatalytic Water Oxidation

Cobalt-based complexes also range from mononuclear to multinuclear systems, representing a promising direction in water oxidation catalysis due to their diverse structural motifs and remarkable electrochemical performance. Their history is more recent compared with manganese, ranging from 2011 to date, with the largest work devoted to mononuclear complexes where ligand design has an important role to control both stability and activity of catalytic species and reaction intermediates.

Cobalt based Cubane Analogues: Dismukes and collaborators[65] synthesized a Cubane $[Co_4O_4(OAc)_4(py)_4]$ complex with four bidentate acetate and four monodentate pyridine ligands, analogous to the Mn-based oxygen-evolving

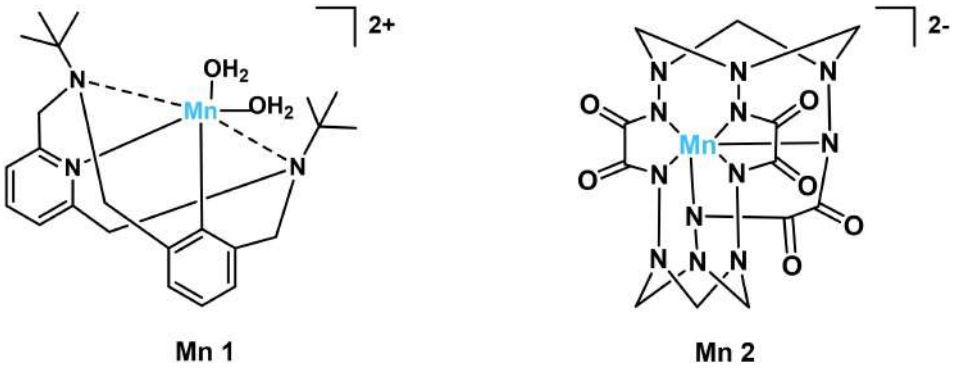

Figure 1. On the left: **Mn 1**, Tetradentate mononuclear Mn complex from Li group; on the right: **Mn 2**, Hexadentate Mononuclear Mn complex from Lin group.

complex previously described. This system undergoes photochemical and electrochemical oxidation, with Density Functional Theory (DFT) studies highlighting Co^{IV} intermediates as pivotal species during catalysis.[66] Furthermore, putative $Co^{IV}=O$ intermediate was spectroscopically measured in Co_4O_4 system under catalytic conditions by Ezhov and co-workers.[67]

Dinuclear cobalt systems:[68] Llobet and co-workers developed a dinuclear cobalt complex with a μ-1,2-peroxo motif stabilized by bis(2-pyridyl)-3,5-pyrazolate (bpp^-) and terpyridine (trpy) ligands; $[Co^{III}_2(trpy)_2(\mu\text{-}bpp)(\mu\text{-}1,2\text{-}O_2)]^{3+}$. This system, inspired by the structural complexity of the Ru-based Blue Dimer, demonstrated distinct vibrational features in resonance Raman spectroscopy, confirming the formation of superoxide intermediates. This design emphasizes the thermodynamic and kinetic benefits of multinuclear arrangements. The same group expanded the scope introducing electronically rich bis(N-methyl-imidazolyl)-pyridine (Me_2bimpy) ligands, which enabled water oxidation at significantly reduced potentials. Lately in 2014, an N-donating cobalt-based dinuclear complex, $[Co_2(\mu\text{-}OH)_2(OH_2)_2(DPFN)](NO_3)_4$ was studied in $Na_2[B_4O_5(OH)_4]$ or $NaBF_4$ buffer. It caused a shift in the observed redox events, providing evidence of the interaction between the electrolyte and the metal complex. Additionally, a pH-dependent characteristic was observed for the complex: above pH 6.5, two overlapping irreversible $1e^-/1H^+$ oxidation events were recorded. These results suggested the potential conversion of one Co^{III} metal center to a higher oxidation state, Co^{IV}. However, when the pH was lowered to acidic conditions, the current dropped to zero, indicating that the catalyst was only active under basic conditions.

Mononuclear Cobalt Complexes: Nocera et al.[69] reported cobalt corrole complexes that enable single-site water oxidation. Functionalized with β-octafluoro and meso-pentafluorophenyl substituents, these complexes exhibit enhanced catalytic properties due to their ligand environment. The "hangman" effect, which involves pendant groups facilitating proton-coupled electron transfer (PCET), and ligand fluorination (**Co 2** in Figure 2) contribute to an overpotential of 580 mV and TOF of 0.81 s^{-1}.

This hangman effect was revisited by Cao et al.[70] tuning proton-accepting ability in cobalt corroles by employing different acid/base pendants including Br, COOH, $PO(OH)_2$ $CH_2PO(OH)_2$.

In line with the hangman effect, the catalytic performance of those cobalt complexes for water oxidation has the order of **Co 6 > Co 5 > Co 4 > Co 3**, indicating that the rate determining step of O–O bond formation during the electrocatalytic water oxidation process is enhanced by basic pendant groups that can facilitate proton transfer.

Berlinguette and collaborators[71] introduced a cobalt complex coordinated by the Py5 ligand (2,6-[bis(bis-2-pyridyl)methoxy-methane]pyridine) (**Co 7**), also known as $[Co(Py_5)(OH_2)]^{2+}$, which displayed distinct redox waves corresponding to Co^{III}/Co^{II} and Co^{IV}/Co^{III} couples. This species can then undergo further reaction to release O_2 and regenerate the starting Co^{II} aqua species. This system involves a PCET process, with a notable pH dependency that underscores its mechanistic intricacies. Quantum chemical models revealed an intermediate-spin quartet state in the Co^{IV}-oxo species, providing insights into its high catalytic efficiency. At pH > 10.3, the redox event shifts toward a PCET process of the $[Co^{IV}\_O]^{2+}/[Co^{III}\_OH]^{2+}$ couple. This results in a nucleophilic attack of water or OH^- on the Co^{IV}-oxo intermediate (Figure 3).

Additional examples include Das' Biuret-modified tetraamidomacrocyclic cobalt complexes (**Co 8–10** in Figure 2),[72] which operate efficiently at basic pH, forming high-valent Co-oxo intermediates.

Porphyrin ligands were employed also to develop cobalt MWOCs, specifically the homogeneous cationic cobalt por-

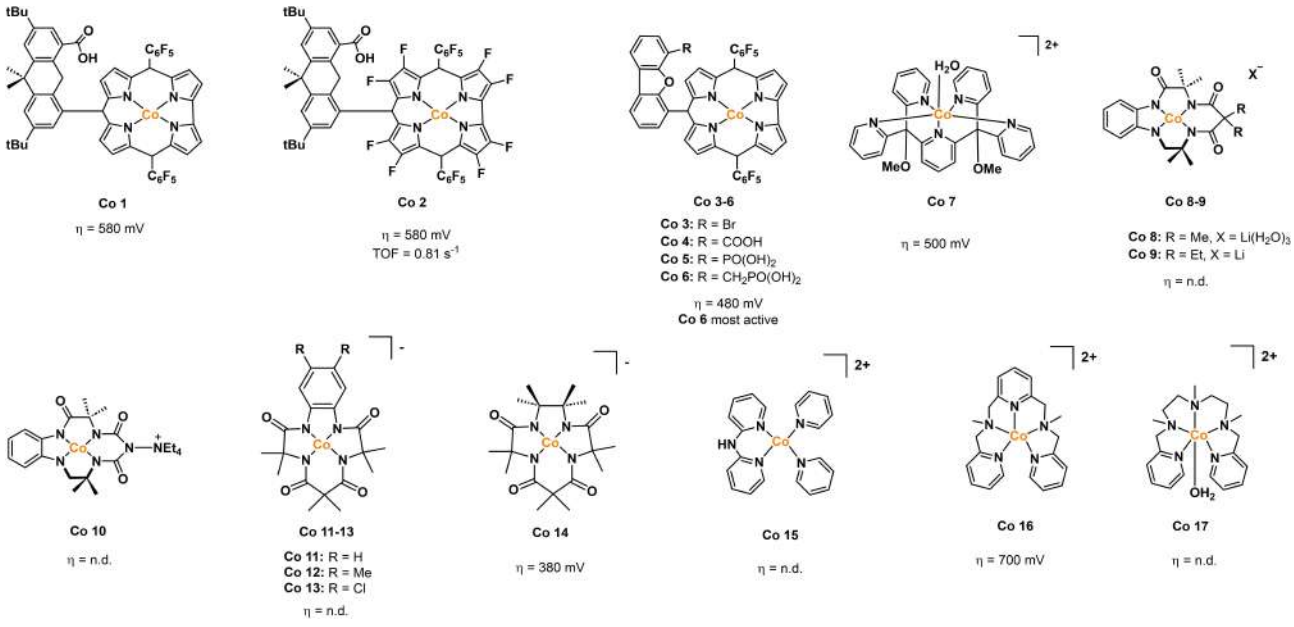

Figure 2. Mononuclear Co complexes **Co 1–17**, bearing nitrogen donor ligands, active in the electrocatalytic oxidation of water.

phyrin complex Co^{II}-TDMImP (where TDMImP is 5,10,15,20-tetrakis-(1,3-dimethylimidazolium-2-yl) porphyrin, was studied by Groves and colleagues[73] and exhibits interesting chemical and electrochemical characteristics: it is water soluble, stable under catalytic conditions, pK_a of the buffer significantly affects the onset potential for water oxidation. Buffers with higher pK_a values reduce the required oxidation potential. Kinetic studies identified PCET during the O–O bond formation as the rate determining step in the catalytic process. This catalyst generates molecular oxygen at a rate of 170 nmol cm^2 min^{-1} ($k_{obs} = 1.4\times10^3$ s^{-1}) with FE close to 90 %.

Cobalt(III) complexes derived from various redox-active non-innocent tetraamido(4−) macrocyclic ligands (TAML) **Co 11–13** (Figure 2) recently demonstrate to electrocatalyze water oxidation at neutral pH.[74]

The redox-active ligands within these complexes assist in the multielectron transfer process by facilitating PCET. Mechanistic insights were provided through a combined approach of DFT calculations and kinetic analyses. The proposed mechanism initiates with a ligand-centered ($2e^-/H^+$) PCET oxidation to form Co^{III}-OH, followed by another PCET step to generate the active $Co^{IV}=O$ intermediate. This intermediate then combines with water to form a peroxide intermediate, which undergoes oxidation to release dioxygen and regenerate the catalyst (Figure 4).

As previously stated, confirming that the molecular complex is the real active species, discrediting the possibility of heterogeneous deposition on the electrode, is relevant for understanding the real mechanism and the actual role of the complex as catalyst or pre-catalyst. In recent advances, a nice study from Hetterscheid's group reported on a deep characterization that demonstrates that the MWOC **Co 15** (Figure 2), namely [Co(HL)] (HL = N,N-bis(2,2′-bipyrid-6-yl)amine), actually works as a stable molecular catalyst.[75] The catalyst revealed reversible and irreversible redox behaviors in a pH 7 phosphate buffer. Cyclic Voltammetry (CV) analysis indicated a $Co^{II}/^{III}$ redox couple at 0.54 V and an irreversible oxidative wave at 1.28 V ascribable to redox activity of the ligand itself, followed by a catalytic wave. The process was found to be diffusive. A comparison between [Co(HL)] electrocatalytic data with those previously reported by Nocera group,[76] which employed a Co^{2+} ($Co(NO_3)_2$ in a sodium phosphate buffer) as source for heterogeneous Co–Pi formation. Although Co–Pi deposition demonstrate to be better in electrocatalytic efficiency, recording a 10 times higher current at 1.6 V versus NHE and FE of 100 % (overpotential 410 mV, 1 mA cm^{-2}), [Co(HL)] FE of 83 ± 6%, is in agreement with homogeneous Co- based catalysts, for which it is more difficult to achieve complete FE due to the diffusion of partly oxidized species before these can turnover. These findings, together with bulk UV-vis measurements and electrochemical quartz crystal microbalance (EQCM) experiments combined with Chronoamperometry, X-ray Photoelectron Spectroscopy (to check the absence of Co–Pi electrode deposition), ^{31}P NMR experiments or trapping experiments with the addition of ethylenediaminetetraacetic acid (EDTA) (to check the presence of free Co^{2+}) highlight that [Co(HL)] remains intact after

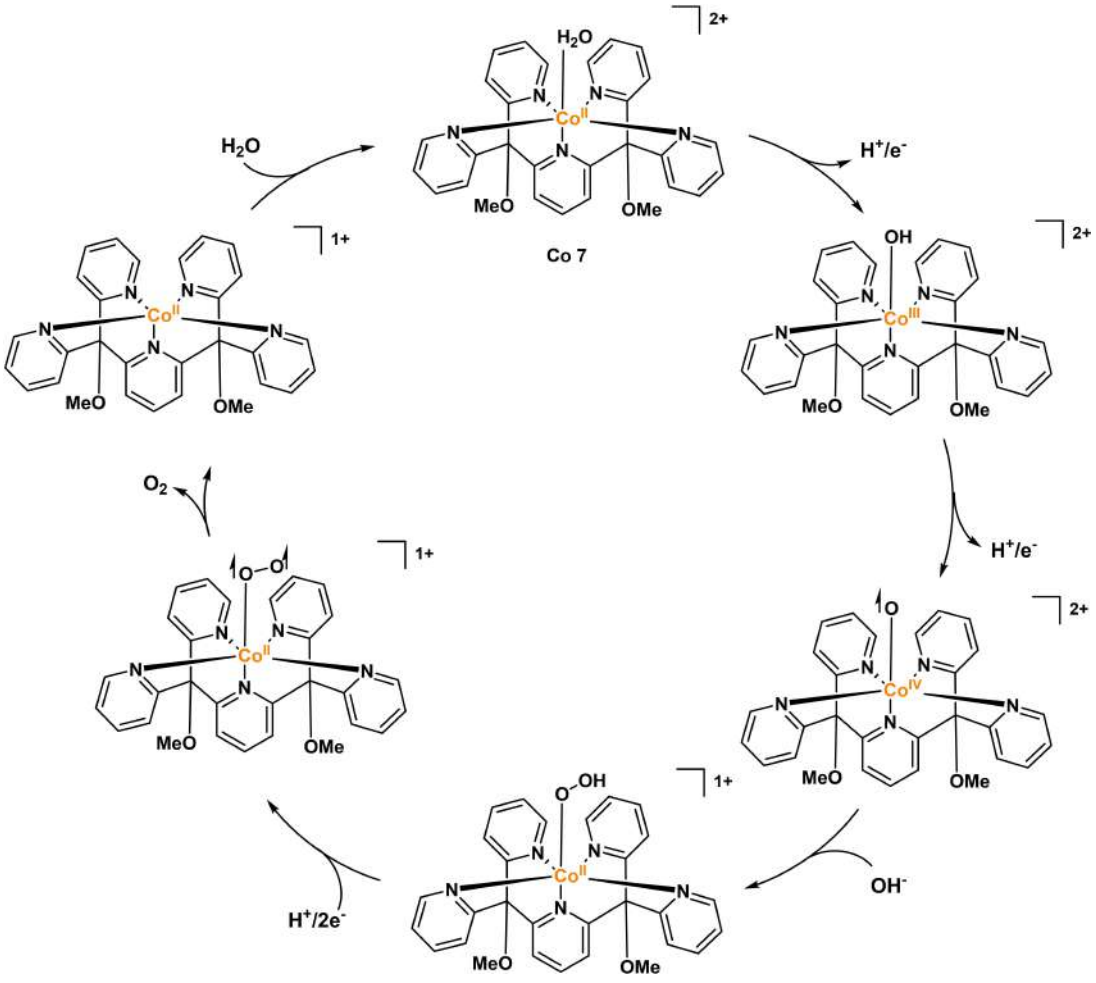

Figure 3. Mechanism for the electrocatalytic oxidation of water catalyzed by Py5 Cobalt complex **Co 7**.

extended electrolysis, supporting its stability as a homogeneous catalyst for water oxidation.

In 2023 Lin and co-workers,[77] employed pentadentate amine-pyridine cobalt complexes $Co(N2Py3)_2$ (**Co 16** in Figure 2) and $Co(N_3Py_2)(OH_2)_2$ (**Co 17** in Figure 2) with slightly different stabilizing ligands in order to reveal their peculiar role. Complex **Co 16** with three-pyridine ring structure, exhibited high FE and good stability. On the other hand, complex **Co 17** bearing an azaalkyl substituent instead of one pyridine showed lower catalytic activity. Electrochemical studies in phosphate-buffered saline at pH 11.0 demonstrated that complex **Co 16** undergoes a ligand oxidation process, forming a $[L_1(Co^{III}\text{-}O)]^{2+}$ intermediate, which can then be converted to the $[L_1(Co^{IV}=O)]^{2+}$ species. In comparison, complex **Co 17** required a mechanism that does not involve the ligand with a redox role. Thus, consecutive oxidations of the cobalt center to form active $[L_2(Co^{IV}=O)]^{2+}$ intermediates is needed. CV measurements of complex **Co 17** showed an oxidation peak at 0.79 V vs. NHE and a catalytic wave at 1.28 V, with a corresponding onset overpotential of 700 mV for water oxidation. Complex **Co 17** exhibited a weaker catalytic current under similar conditions, reinforcing the superiority of complex **Co 16** in this reaction. Long-term electrochemical tests, such as controlled potential electrolysis (CPE), revealed that complex **Co 17** maintained a stable catalytic current density of approximately 0.65 $mA\,cm^{-2}$ after initial fluctuations, indicative of its robust catalytic performance. In contrast, complex **Co 17** exhibited a significantly lower catalytic current of 0.11 $mA\,cm^{-2}$, further confirming its reduced activity. The FE for oxygen production was 96% for complex **Co 16**, with a total oxygen yield of 22.1 mmol. Complex **Co 17**, on the other hand, exhibited FE of 97%, but with a significantly lower oxygen yield of 4.5 mmol. Differential pulse voltammetry (DPV) was employed to clarify the redox processes and catalytic mechanisms of both complexes. For complex **Co 16**,

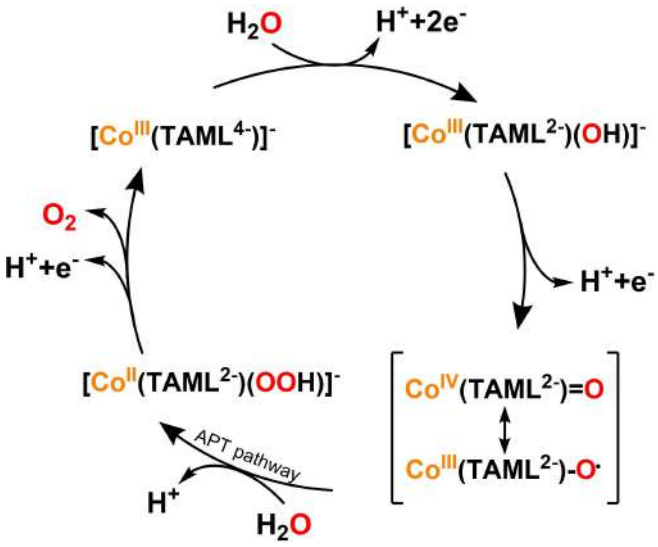

Figure 4. Proposed mechanism for Co-TAML (**Co 11–13**) complexes.

the first oxidation step corresponded to the Co^{II}/Co^{III} couple at 0.69 V, followed by ligand oxidation at 1.15 V. For complex **Co 17**, the first oxidation occurred at 0.61 V, with the second step at 1.17 V, attributed to the oxidation of the Co^{II} center rather than the ligand.

The study underscores the importance of ligand structure in modulating the redox properties of cobalt complexes and their catalytic efficiency in water oxidation. The redox-innocent N_2Py_3 ligand in complex **Co 16** enables efficient electrochemical water oxidation via a ligand-assisted mechanism, whereas the similar N_3Py_2 ligand in complex **Co 17** leads to less reactive intermediates and lower catalytic activity. This work contributes valuable insights into how ligand design can be optimized to enhance the stability and catalytic activity of MWOCs.

4.3. Copper Complexes for Electrocatalytic Water Oxidation

Dinuclear copper complexes: A recent study from Wang et al. analyses the comparison between mononuclear and dinuclear copper complexes bearing tetradentate nitrogen ligands (Figure 5).[78] The superior activity of the dinuclear complex **Cu 2** – Figure 5 (TOF of 144 s^{-1} vs. 4.86 s^{-1} for **Cu 1** – Figure 5 - at pH 12) has been ascribed to a unimolecular two-site mechanism, where both copper centers cooperate to stabilize the charge and facilitate the formation of the O–O bond complex. XPS data suggest that a small amount of CuO_x may form on the electrode during prolonged electrolysis, although SEM images show no clear deposition.

A Similar dinuclear catalyst **Cu 3** was previously reported by Zhang et al.[79] who already stated its competitive stability

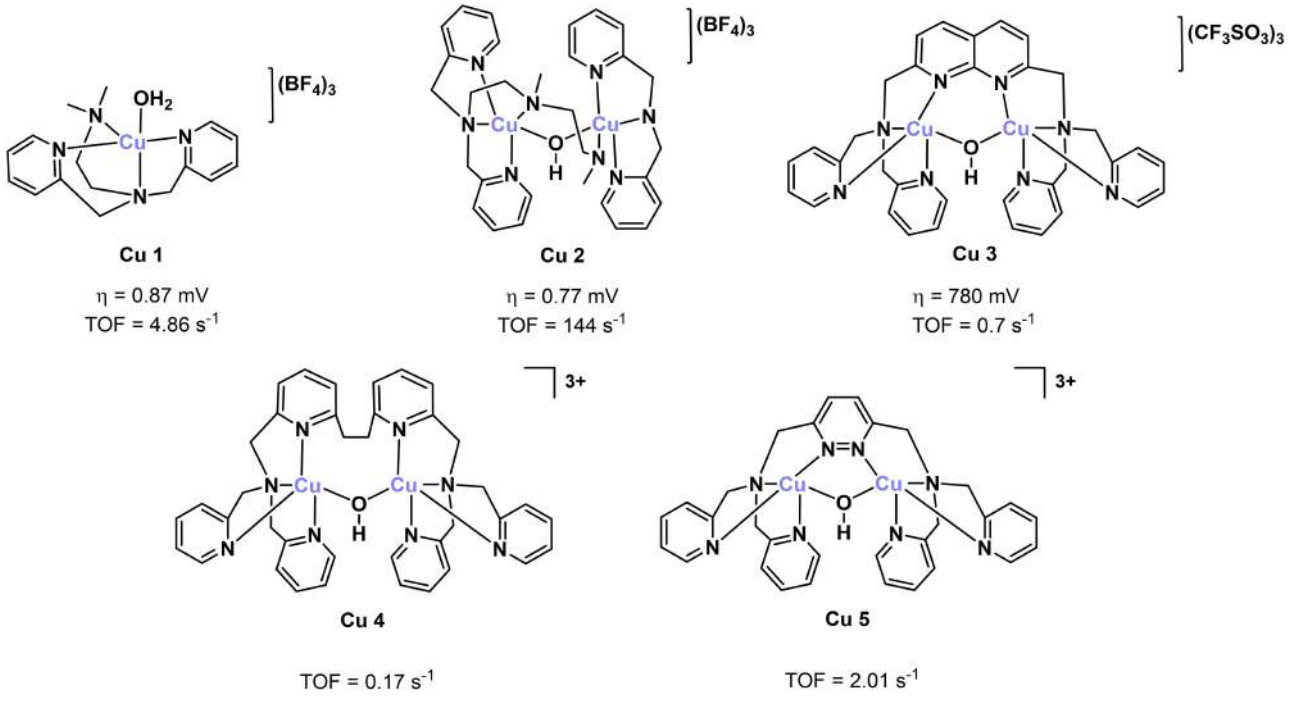

Figure 5. Mononuclear **Cu 1** and dinuclear complexes **Cu 2**-**Cu 5**. Counteranion for complexes **Cu 4–5** is ClO_4^-.

and catalytic activity (overpotential 780 mV, TOF 0.7 s^{-1}) under neutral conditions (phosphate buffer – pH 7). Even in this case O–O bond formation occurs via cooperative bimetallic activation of the copper centers, unlike mononuclear systems, which require high oxidation states for copper (Cu^{IV} or Cu^{III}) (**Cu 1(CF_3SO_3)$_3$** at pH 7 overpotential of 970 mV and a lower TOF of 0.1 s^{-1}).

Recently, research interest in dinuclear copper complexes for water oxidation has been revitalized by the group that pioneered and elucidated **Cu 3** reactivity.[80]

Comparison between **Cu 3-Cu 5** show an enhancement in catalytic activity strictly related with the increased rigidity. In phosphate buffer solution (PBS, 0.1 M, pH 7.0), electrocatalytic behaviour of **Cu 4**, bearing a 1,2-di(pyridin-2-yl)ethane linker, corresponds to a lower TOF of 0.17 s^{-1} (0.7 s^{-1} for **Cu 3**). On the other hand, the dicopper center with the most rigid pyridazine linker (**Cu 5**) exhibits significantly faster catalytic rate (2.01 s^{-1}). Mechanistic investigations show that O–O coupling takes place between a terminal Cu^{III}-OH and a bridging μ-O* radical, nicely demonstrating the critical role of spatial geometric needed to align with the O–O bonding.

This study, which also presents a comparative analysis of the distinct behavior of analogous iron complexes (examined in the dedicated iron section), further underscores the significance of rational design, with a particular focus on geometric considerations, in enhancing water oxidation efficiency.

Mononuclear copper complexes: First appearing in 2012, with Mayer work[81] a Copper(II)-based 2,2′-bipyridine water oxidation catalyst [(bpy)Cu(μ-$OH)_2$] demonstrated pH-dependent catalytic activity, operating effectively within an alkaline range of pH 11.8 to 13.3. A promising TOF of 100 s^{-1} is accompanied by high overpotential of around 750 mV and poor stability. Later on, Lin and Papish explored multiple modified versions of Mayer's complex using 6,6′-dihydroxy-2,2′-bipyridine ligands. Hydroxy functionalization, although lowering the overpotential (477-530 mV) and favoring the overall stability, was detrimental for the turnover of the reaction (TOF 0.4 s^{-1}).

Other mixed ligands bearing nitrogen and oxygen donor sites are also suitable for stabilizing Copper(II) complexes allowing further variations in electronic properties of electrocatalytic water oxidation catalysts. In 2015 [Cu(pyalk)$_2$] (**Cu 6** in Figure 6, with pyalk = 2-pyridyl-2-propanoate, KNO_3/KOH at pH 10.4) complexes, have been prepared by deprotonation and bind directly to the copper.[82] This chelation effect helps stabilize the metal in high oxidation states, crucial for electrocatalysis. **Cu 6** exhibits electrocatalytic water oxidation with an overpotential of 580 mV and TOF of 0.7 s^{-1}. Notably, the complex remains stable for over 12 h during bulk electrolysis at 1.1 V vs. NHE.

Deprotonatable 2-(2'-pyridyl)-imidazole copper complex **Cu 7** developed by Warren et al. in 2017[83] exploits the non-innocent nature of the 2-(2'-pyridyl)-imidazole (pimH) ligand, which enhances the electron density at the copper center, facilitating its oxidation. Working in 0.1 M NaOH/NaOAc at pH 12, the system results in a catalytic rate of 35 s^{-1} and an overpotential of 300 mV for electrocatalytic water oxidation, making it an efficient catalyst.

Lately Ghosh's report[84] on peptide-based copper WOCs (0.1 M phosphate buffer at pH 11.5), such as **Cu 8**, emphasized the importance of intramolecular cooperative catalysis. Indeed, **Cu 8** showed an impressive FE of 91% over 15 h of bulk electrolysis, despite the high overpotential of 800 mV and a relatively low TOF of 5.8 s^{-1} the overall efficiency makes this complex of interest for future ligand design and development. Indeed, hydroxyl group in the second coordination sphere is likely to stabilize high-valence intermediates and support efficient PCET during the reaction.

Interesting behavior was also demonstrated by Reglier et al. in 2018 for the tridentate bis-acqua complex [(RPY_2)Cu-(H_2O)$_2$] (**Cu 9** in figure 6).[85] This complex operates in $NaNO_3$ at pH 7 at a relevantly low overpotential of 280 mV

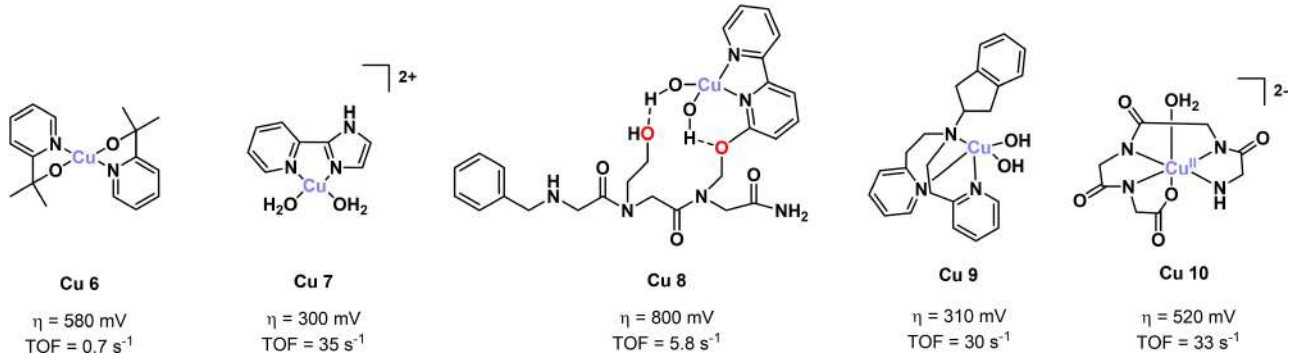

Figure 6. Copper complexes bearing nitrogen and oxygen donor ligands **Cu 6–10**.

in neutral aqueous solutions, although with limited efficiency. Nevertheless, this report exemplifies how in-depth characterization can elucidate complex reactivity and catalytic mechanisms. Indeed, potentiometric titrations, spectroscopic studies (^{19}F NMR, UV-vis) and DFT calculations allowed to follow the complex speciation, its pH dependency and stability constants. At pH 3.0, free copper is predominant (80 %). Then, increasing the pH, the copper complex with a monoprotonated ligand is likely to occur. At pH > 5, the fully deprotonated ligand is bound to Cu^{II} with three nitrogen donor atoms (**Cu 9**). This species, being predominant between pH 5 and 7 (> 80 %), is the one active in electrocatalytic water oxidation, which proceeds via mononuclear copper species, with a $1H^+/2e^-$ process identified as the rate determining step. At pH > 7.0, another species, probably deriving from loss of one proton from a bound water molecule, is identified. The last deprotonation was finally above pH 8.5 again derived from an external copper-bound water molecule. At pH > 9.0, precipitation occurs. For further details on the interesting reactivity of the different species identified inactive in WOC, the reader is invited to examine in dept the Reglier's group work.

A pentadentate bis-pyridyl dicarboxamide ligand, introduced in 2014, by Meyer[86] and colleagues in a new copper(II) complex, (Cu^{II}- N,N-bis(2-(2-pyridyl)ethyl)pyridine-2,6- dicarboxamidate [Cu^{II}-Py_3P]) operates in phosphate buffer (pH 8) via a single site mechanism, with the formation of a Cu^{III} intermediate involved in the oxidation process (overpotential 640 mV, TOF 30 s^{-1}). Same group also explored a copper(II) complex based on a triglycylglycine (TGG) macrocyclic ligand (**Cu 10** in Figure 6),[87] $[(TGG_4)Cu^{II}-OH_2]^{2-}$ (pH 11, overpotential 520 mV, TOF 33 s^{-1}) The complex showed excellent stability during electrolysis, with FE of nearly 100 % over extended periods, highlighting its potential for use in sustained electrocatalytic water oxidation. This complex demonstrated a well-defined catalytic cycle, beginning with the oxidation of Cu^{II} to Cu^{III}, followed by oxidation to Cu^{IV} and the formation of peroxide, which subsequently decomposed to yield molecular oxygen as depicted in Figure 7.

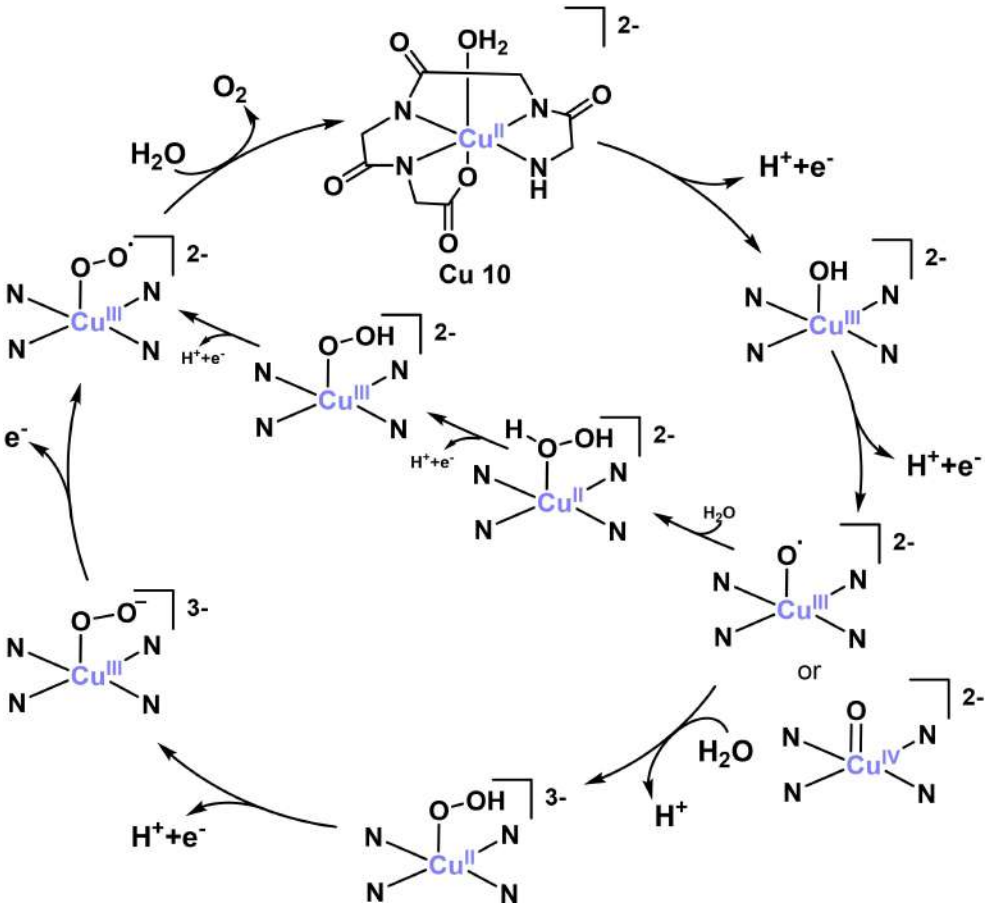

Figure 7. Proposed catalytic cycle for Copper(II) molecular electrocatalyst **Cu 10**.

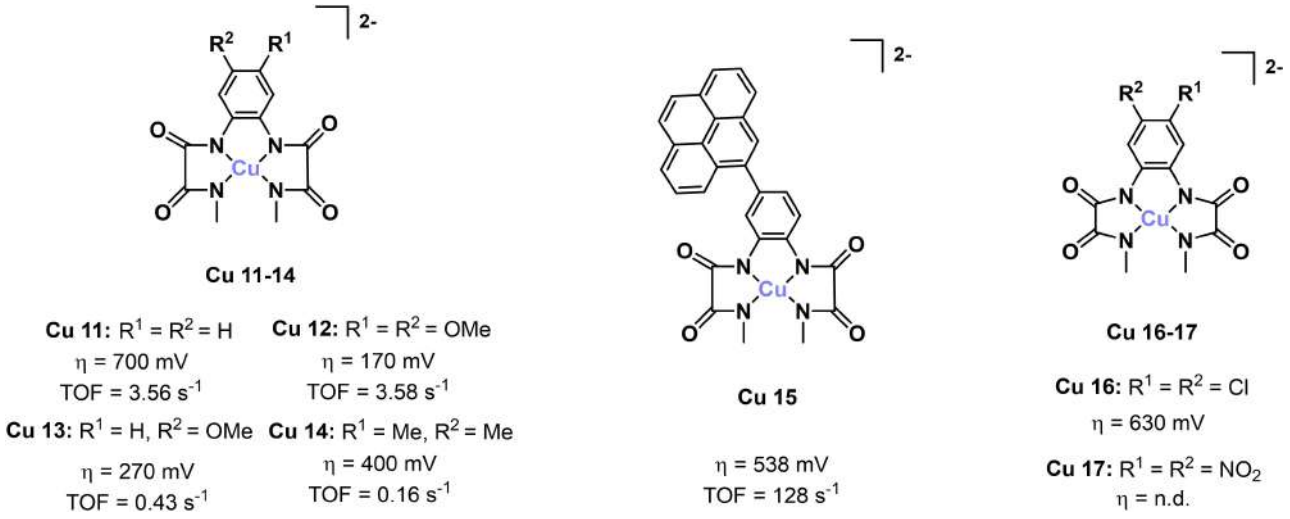

Figure 8. Mononuclear Copper complexes employed as water oxidation electrocatalysts. Countercation for complexes **Cu 11-Cu 14** is NMe_4^+, for complexes **Cu 15–17** is PPh_4^+.

In 2015 Llobet and colleagues[88] expanded the research on the use of copper tetradentate complexes featuring o-phenylene bis(oxamidate) ligands (tetraanionic amidate ligands, N1,N1'-(1,2-phenylene)bis (N2-methyloxalamide)) **Cu 11–14** in Figure 8. Remarkably, these complexes (working in phosphate buffer at pH 11,5) allowed a large tunability of overpotential which range from 700 mV for $R_1 = R_2 =$ H (**Cu 11**) to 170 mV for $R_1 = R_2 =$ OMe (**Cu 14**) and of, on the other way around, turn over frequencies (3.56 s^{-1} for **Cu 11** vs 0.16 s^{-1} for **Cu 14**), demonstrating a non-innocent behaviour of the tetradentate ligand. Additionally, in the same vein, pyrene-functionalized copper catalyst,[89] such as **Cu 15** (Figure 8), although demonstrating an intermediate overpotential (538 mV), better performs with an enhanced catalytic activity (TOF = 128 s^{-1}) due to the increased π-delocalization provided by the pyrene modification. Interestingly, the pyrene functionalization has been exploited in order to support the catalyst on graphene support. Indeed, the immobilized catalyst showed a significant increase in TOF (k_cat (TOF) = 540 s^{-1}), underlining the importance of π-π stacking interactions for improving catalytic efficiency in heterogeneous systems.

Reactivity studies and DFT calculation allowed to propose the catalytic stages of the reaction, as summarized in Figure 9.

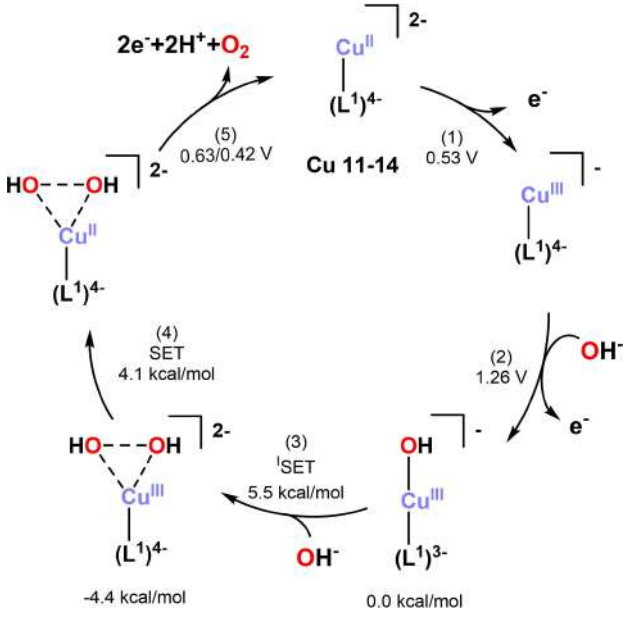

Figure 9. Calculated catalytic cycle for Llobet's copper complexes **Cu 11–14** active in electrocatalytic water oxidation. Free energy changes for steps at the electrode are in volts (red) and for steps in solution in Kcal/mol (blue).

Recent developments identify an updated interest in oxamidate complexes, introduced above with the pioneering work of Llobet and coworkers,[88,89] as promising ligands for the copper catalyzed MWOCs. In fact in 2021, Chattopadhyay and colleagues,[90] extended the family of **Cu 11–14** copper(II) complexes with tetraanionic amidate ligands to derivatives with electron-donor substituents (**Cu 16–17**) stabilized by PPh_4^+ counteraction. In this latter work previously proposed catalytic cycle reactive intermediates species, has been verified by spectroscopic signature by means of *in-situ* electron paramagnetic resonance (EPR), FT-IR, and rR (resonance Raman) spectroelectrochemical studies accompanied by further DFT calculation. This nicely helped to confirm the elementary chemical and electrochemical events toward the O_2 formation. The copper(II) o-phenylene bis-oxamidate complexes reactivity has been thus definitely recognized as a function of the substitution pattern on the

periphery of the aromatic ring with a ligand-centered oxidation (to a radical species) preferred over metal-centered one. rR spectroelectrochemical study revealed a superoxide species, under catalytic conditions, which provides the evidence for the O – O bond formation during OER. CV analysis and DFT studies confirmed that the rate determining step concerns the generation of the radical oxidized ligand species and its reaction with OH^-.

Nitrogen tetradentate ligands based Cu^{II} complexes were concurrently developed in 2015 by Pap, Szyrwiel, Malinka et al.[91] exploiting tetrapeptide ligands as for **Cu 18** and **Cu 19** complexes (Figure 10).

Investigated at pH 11 (phosphate buffer), the positioning of the equatorial histidine in the copper complex **Cu 19** enhances the TOF to 53 s^{-1} (vs 24 s^{-1} for **Cu 18**), while maintaining a similar overpotential, likely due to a favorable proton–π interaction. In particular, the substitution of glycine in the ligand of **Cu 18** with a proton-accepting histidine in **Cu 19** is likely to facilitate PCET pathways during redox processes thanks to the interaction of protons with the lone pair of the amine group in the terminal histidine residue. Following the promise of tetradentate copper complexes, in 2016 Cu^{II} tetraazacyclotetradecane complexes were tested by Sun et al.[92] Working under neutral conditions, the macrocyclic ligand stabilizes copper-oxo intermediates, although with lower performances if compared with other complexes above described.

Promising results have been instead found exploiting a tetradentate porphyrin based Cu^{II} complex. Indeed, Tetrakis(4-N-methylpyridinium) Cu^{II}-porphyrin complex (**Cu 20** in Figure 10),[93] demonstrates electrocatalytic water oxidation at an overpotential of 313 mV and a current density of 0.1 mA cm^{-2} working phosphate buffer at pH 7. Furthermore, under acidic conditions (pH 3), the complex shifts from oxygen to hydrogen peroxide production, indicating a unique two-electron transfer pathway for peroxide formation.

Later on, in 2023 Hetterscheid extended his research to polypyridyl ligands previously employed in cobalt MWOC active complexes, to develop a novel tetradentate copper complex, which also favors a radical-oxo coupling during catalysis.[94] Although the efficiency of the catalytic system is not specified, the study stated that the use of redox-active ligands facilitates electron delocalization within the ligand's π system.

In 2024, Naskar et al.[95] reported highly efficient Cu^{II} complexes with bis-amide ligands of o-phenylene diamine complexes $[Cu^{II}(L1)]$,$[Cu^{II}(L2)(H_2O)]$, and $[Cu^{II}(L3)]$ [bis-amidetetradentate ligands: L1 = N,N'-(1,2-phenylene)dipicolinamide,L2 = N,N'-(4,5-dimethyl-1,2-phenylene)bis(pyrazine-2-carboxa-mide), L3 = N,N'-(1,2-phenylene)bis(pyrazine-2-carboxamide)], which work at pH 13. Although affected by a high overpotential 697 mV, the catalytic system achieves a TOF values as high as 1462 s^{-1} for $[Cu^{II}(L2)(H_2O)]$. The enhanced performance was attributed to the stabilization of the Cu^{III}-ligand radical cation transition state, facilitated by electron-donating groups in the ligand, which lowered the activation barrier for water oxidation. This finding further demonstrated the potential for high-efficiency copper-based catalysts with fine-tuned ligand structures for electrocatalytic applications.

In a very recent inspiring paper, Llobet and coworkers exploited, as an evolution of their own work previously explored on the importance of π- π stacking for heterogenization techniques,[89] polypyrene amidate copper complexes

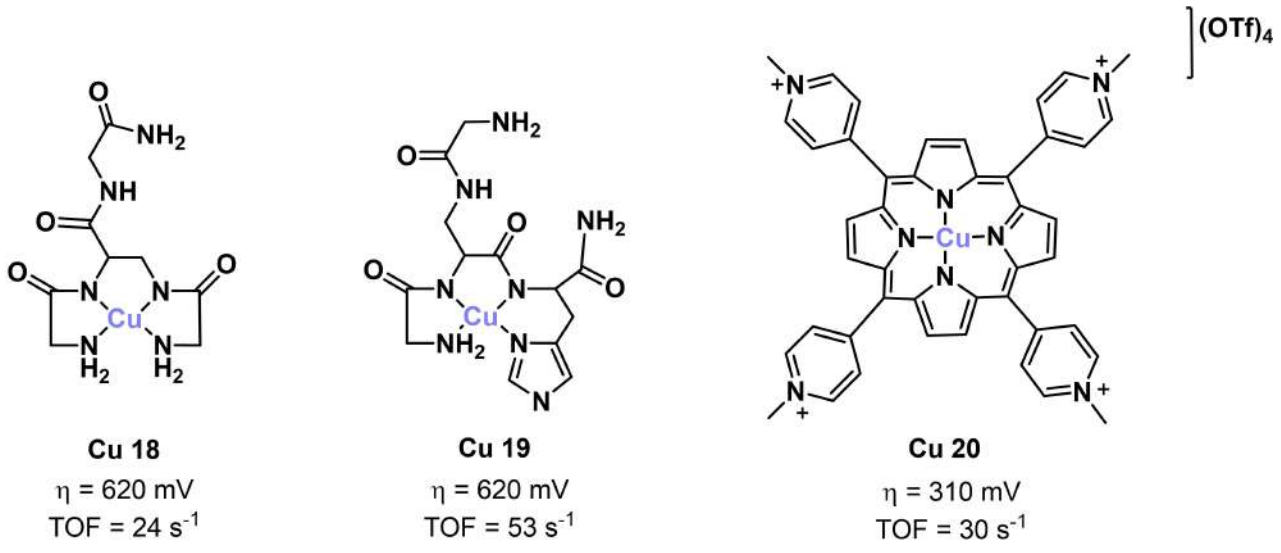

Figure 10. tetrapeptide and porphyrin as ligands in copper-based catalysts **Cu 18–20** for electrocatalytic water oxidation.

(**polyCu 21** in Figure 11) for their immobilization on indium thin oxide (ITO) electrodes.[96] In terms of anchoring methodologies, molecular redox catalysts are linked to surfaces either through covalent or noncovalent bonds. Noncovalent interactions, such as $\pi-\pi$ and $CH-\pi$ interactions avoid the need for ligand modifications. Regarding electropolymerization, the complexes were polymerized on nano-ITO/ITO electrodes by cyclic voltammetry within a potential range of −0.8 to $^{+}$0.8 V vs. Fc/Fc^{+}, generating a stable polymer that anchors firmly to the electrode surface (Figure 11).

In aqueous solutions, redox studies (pH 7.5, 9, and 10) showed metal-based redox events, with the Cu^{III}/Cu^{II} couple being dominant. A significant electrocatalytic wave, indicating water oxidation, was observed at a potential onset of 0.8 V vs. NHE, achieving current densities of 0.4–0.5 mA cm^{-2} at 1.3 V. This hybrid materials serve as molecular anodes in water oxidation catalysis achieving current densities of 400–500 μA cm^{-2} at pH 10, with overpotentials ranging from 560–720 mV at neutral-basic pH. Although these materials showed limited stability, and further studies are ongoing to improve their performance and stability, Llobet research paves the way for electrocatalytic Hybrid MWOC systems which can be designed for application in photoelectrochemical (PEC) devices.

Following the interest in tetraamide copper complexes for electro polymerization, the same research group has been working on a new alkyl-thiophene functionalized tetra-amidate ligand:[97] (**Cu 22** in Figure 12) This complex exhibits electrochemical characteristics like the previous pyrene-functionalized systems.

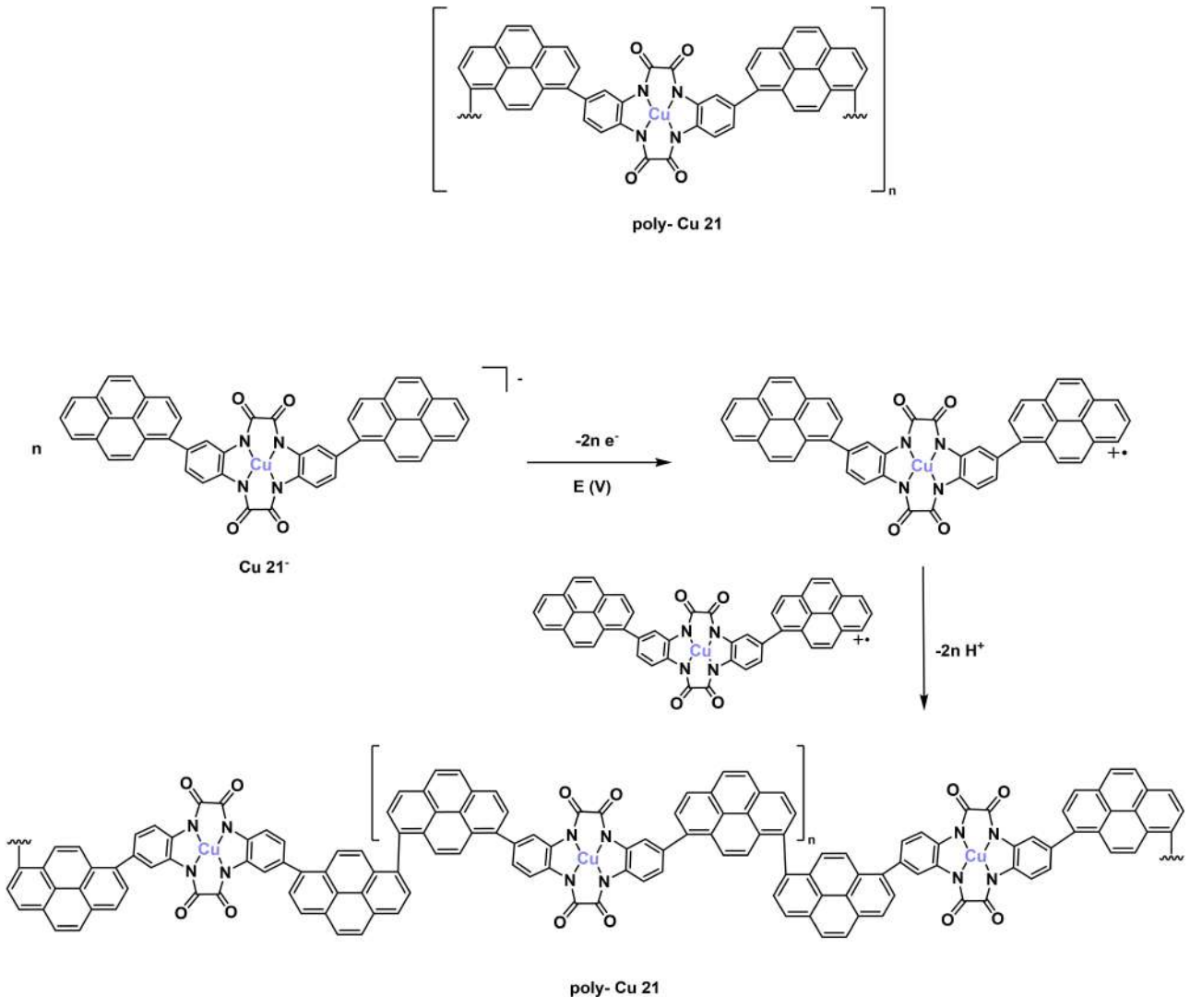

Figure 11. Electropolymerization of **Cu 21**$^{-}$ to generate **poly-Cu 21**.

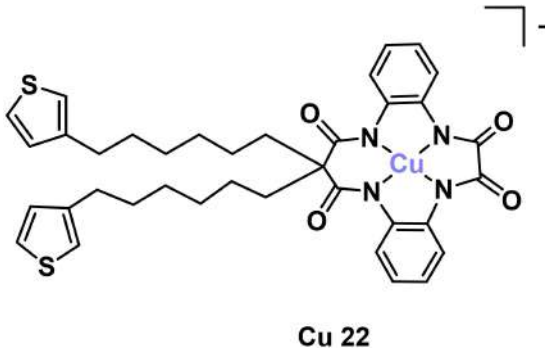

Cu 22

Figure 12. Monomeric thiopene functionalized tetraamide complex **Cu 22**.

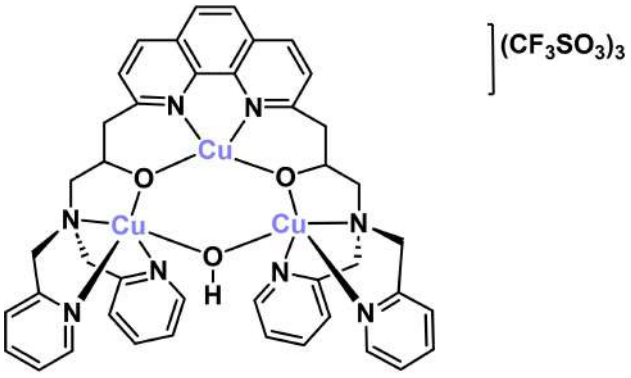

Cu 23

Figure 13. Molecular structure of the tricopper core in the $[(app^{2-})Cu^{II}_3(\mu\text{-}OH)]^{3+}$ catalyst **Cu 23**.

CV in acetonitrile reveals multiple redox events associated with ligand oxidation, while electropolymerization results in the formation of a stable catalyst for water oxidation. At pH 10, it operates with an overpotential of 560–720 mV, showing promise for PEC applications. The hybrid material, GC/CNT@p-**Cu 22** maintained complex integrity and catalytic activity for over 11,000 TONs, as confirmed by techniques including X-ray absorption spectroscopy (XAS). Unlike Fe or Ni oxide-based water oxidation catalysts that require extremely basic conditions, this material works effectively under neutral pH. Its catalytic wave begins at a low overpotential of 250 mV (≈1.07 V), making it more efficient than some of the best Ru-based catalysts, which operate at higher overpotentials of around 450 mV and show TONs over 1 million and TOFs in the range of 10^5 s^{-1} as described in paragraph 3. This work represents the first example of a molecular water oxidation catalyst based on a first-row transition metal complex anchored on a conductive solid support, maintaining its integrity after more than 11,000 TONs.

Interestingly, very high TOF up to 20000 s^{-1}, with an overpotential of 910 mV, was reached in the work of Zhang et al.[98] The group developed a trinuclear copper cluster **Cu23** in Figure 13, formed in $NaHCO_3$ solution (1 M, pH 8.4) exploiting a trinucleating ligand, 2,9-bis{[2-hydroxy-N,N-bis(2-pyridylmethyl)]aminopropanol- 1,10-phenanthroline (H_2app). The isosceles triangular arrangement of the 3 copper in the obtained structure closely resemble the active site of multicopper oxidases (MCOs).[99] Authors stated that bringing three copper centers in close proximity is an advantage for multisite interactions with water leading to O − O bond formation not achievable by mono- or binuclear copper complexes.

4.4. Nickel Complexes for Electrocatalytic Water Oxidation

One of the first nickel-based homogeneous catalysts was developed by Lu and co-workers in 2014,[100] where the metal center was embraced by a nitrogen-donor macrocycle **Ni 1** (in Figure 14). It catalyzes water oxidation at neutral pH in phosphate buffer with an overpotential of 170 mV. A few years later the macrocycle was further modulated by modifying the methylation degree on the cyclen ligand, obtaining **Ni 2** and **Ni 3** (see Figure 14).[101] The mechanism (Figure 14), on the grounds of experimental and computational studies, involves oxidation states between $^{+}2$ and $^{+}4$ and the formation of a peroxide intermediate. The steric effect from methyl groups prevents the formation of inactive nickel(III)-phosphate species. These complexes show a pH- and buffer-dependent decomposition pathway, with NiO_x formation at pH = 7 but not at pH = 6.5. The substitution of the phosphate buffer with bicarbonate leads to a decrease in redox potential for both the Ni^{IV}/Ni^{III} couple and for electrocatalytic water oxidation process, which clearly indicates how bicarbonate is not an innocent axial ligand.

Further investigation have been devoted to demonstrate the role of $Ni^{IV/III}$ intermediates in the O–O bond formation mechanisms. After experimentally excluding intermetallic reactions due to first-order dependence on the concentration of nickel species, other hypotheses such as O–O bond formation by: i) HO-OH coupling, ii) water attack, and iii) O–H insertion have been evaluated by DFT calculation. The HO-OH coupling on the *cis* isomer was finally found as the most feasible O–O bond formation mechanism (ΔG = 24.6 kcal mol^{-1}).

The completely methylated macrocyclic analogue **Ni 4** (Figure 14) was subsequently synthesized by Li et al. in

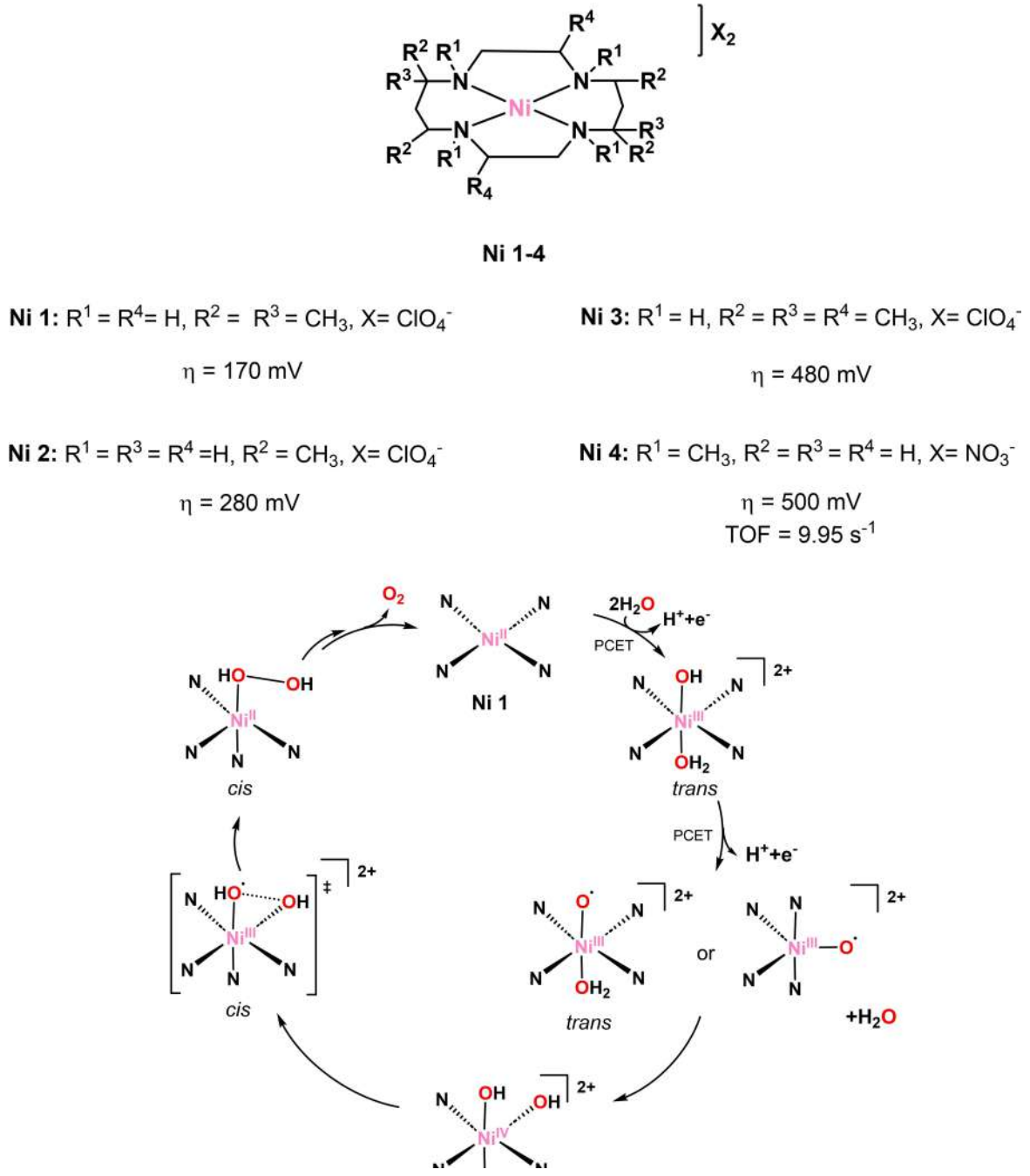

Figure 14. Cyclam complexes of Nickel(II) active **Ni 1–4** in electrocatalytic water oxidation.

2019,[102] which revealed to be a robust catalyst for water oxidation with a moderate overpotential (~500 mV). **Ni 4** operates via a proton-coupled electron transfer mechanism and, although with a higher overpotential (~500 mV at pH 7) with respect to **Ni 1**-**Ni 3**, it exhibits high catalytic activity with record TOF of 9.95 s^{-1}, attributed to the methylation of the macrocyclic ligand, which enhances electron donation to the metal center. Additionally, the catalytic current shows a linear dependence on the proton-accepting ability (pK_a) of the added base, which plays a crucial role in regulating catalytic activity by participating in the key O–O bond-forming step.

The complexes $[Ni^{IV}L(PO_4)_2]^{2-}$ **Ni 5** and $[Ni^{IV}L(CO_3)_2]$ **Ni 6** (Figure 15) still possess the equatorial cyclen ligand but with no methyl groups either on the carbon chains or nitrogen

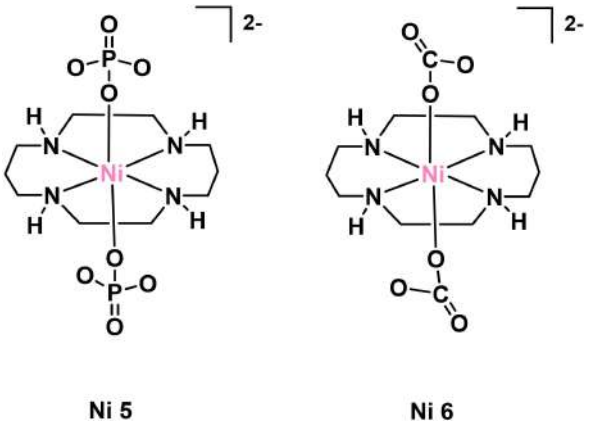

Figure 15. Hexacoordinated Nickel cyclam complexes **Ni 5** and **Ni 6**.

donor atoms, differently from **Ni 1**-**Ni 4**, and this allows the coordination of phosphate and carbonate anions in axial positions stabilizing Ni^{IV} species.[103]

Both **Ni 5** and **Ni 6** exhibit catalytic activity in phosphate and carbonate buffers. Nevertheless, carbonate, unlike phosphate, actively participates in the redox process, facilitating the O–O bond formation through a hydrolysis mechanism. This behavior is consistent with the involvement of the ligated carbonate in the catalytic water oxidation as a non-innocent ligand previously proposed. The mechanism concerns an acid catalyzed O–C bond hydrolysis (Eq. 1) or C–O bond breaking (Eq. 2):

$$[Ni^{IV}L(CO_3)_2] + H_2O \rightarrow [Ni^{IV}L(CO_3)(OH)]^+ + HCO_3^- \quad (1)$$

$$[Ni^{IV}L(CO_3)_2] \rightarrow [Ni^{IV}L(CO_3)(O)] + CO_2 \quad (2)$$

Coupling reaction (Eq. 3) of the products of the previous reactions leads to water oxidation to peroxide, which is liberated upon hydrolysis (Eq. 4):

$$[Ni^{IV}L(CO_3)(OH)]^+ + [Ni^{IV}L(CO_3)(O)] \rightarrow [(CO_3)LNi^{III}O - ONi^{III}L(CO_3)] + H^+ \quad (3)$$

$$[(CO_3)LNi^{III}O - ONi^{III}L(CO_3)] + 2\,H_2O \rightarrow 2\,[Ni^{III}L(CO_3)(OH)] + H_2O_2 \quad (4)$$

A large number of Ni complexes with multidentate ligands, depicted in Figure 16, gave interesting results within the framework of electrocatalyzed water oxidation up to 2020. No more recent advances have been found for this metal.

Porphyrine ligands has been employed by Cao in 2015[104] in the development of water-soluble complex $[Ni(Por\text{-}Hpy_4)]^{4+}$ **Ni 7** (Figure 16) which operates in neutral phosphate buffer (pH = 7) with a TOF of 0.67 s^{-1} at 20 °C. It demonstrates low overpotential (180 mV) and stable electrocatalytic performance over a large pH range (2–8). **Ni 7** operates via a single-site mechanism, mediated by a Nickel(III) hydroxide intermediate, and shows no significant degradation even after 10 h of electrolysis.

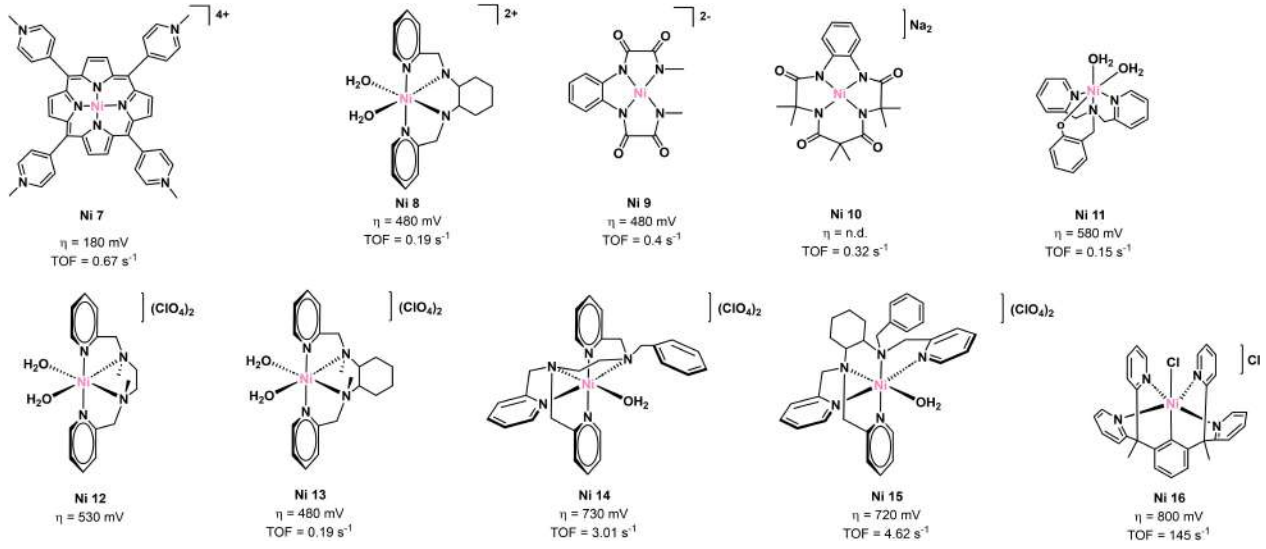

Figure 16. Non-cyclam mononuclear Nickel complexes **Ni 7–16** employed as electrocatalytic water oxidation.

The catalyst $[Ni(L2)(H_2O)_2]$ **Ni 8** (Figure 16, H_2L2 = *N*1,*N*2-bis(pyridin-2-ylmethyl)cyclohexane-1,2-diamine) was reported by T–B. Lu and co-workers in 2016,[105] and it operates in neutral pH with a dual-role of phosphate buffer which participate in PCET during the catalytic cycle. **Ni 8** does not form nickel oxide (NiO_x) deposits during catalysis and shows a pH-dependent performance, with its stability confirmed by electrochemical characterization.

A nickel(II) phenylenebis(oxamidate) complex **Ni 9** (Figure 16) with modulated N/O donor sets were developed by Ding.[106] It exhibits a distinct water oxidation mechanism compared to copper(II)-bis(oxamidate) complexes developed by Llobet's research groups (*see paragraph 4.3*). A single-electron transfer mechanism is observed, while deactivation occurs due to proton transfer in acidic conditions.

The mononuclear hydrosoluble nickel(II) complex bearing the non-innocent tetraamido macrocyclic ligand $TAML^{4-}$, $Na_2[Ni(TAML)]$ **Ni 10** (Figure 16), was reported in 2020[107] and exhibits efficient water oxidation at neutral pH using a phosphate buffer (0.1 mol L^{-1}) under controlled-potential electrolysis (CPE) using an ITO working electrode at 1.75 V (vs. NHE) with no NiO_x formation. The suggested mechanism involves one-electron oxidation of Ni^{II} to Ni^{III} followed by a PCET process, eventually leading to dioxygen evolution. The redox-active nature of the ligand plays a key role in facilitating the catalytic cycle as confirmed by electrochemical and spectroelectrochemical studies, differently from cyclen-type macrocyclic complexes reported above.

The complex $[Ni(L3)(H_2O)_2]^+$ **Ni 11** (Figure 16, HL3 = 2-((bis(pyridin-2-ylmethyl)amino)methyl)phenol) was synthesized by Wang et al.,[108] and operates as catalyst via the formation of a Ni^{III} phenoxyl radical thanks to the redox-active nature of the ligand, showing a TOF of 0.15 s^{-1}. It catalyzes water oxidation at a modest overpotential (400 mV). The use of one phenoxido arm in the ligand instead of only pyridyl moieties represents a fruitful choice that does not allow the formation of high valent nickel intermediates. The presence of coordinated water molecules has been determined to also be crucial for the activity of **Ni 11**.

Labile water molecules are also an important feature in $[NiL4(H_2O)_2](ClO_4)_2$ **Ni 12** and $[Ni(MCP)(H_2O)_2](ClO_4)_2$ **Ni 13** (Figure 16, L4 = *N*1,*N*2-dimethyl-*N*1,*N*2-bis(pyridin-2-ylmethyl)ethane-1,2-diamine, MCP = *N*1,*N*2-dimethyl-*N*1,*N*2-bis(pyridin-2-ylmethyl)cyclohexane-1,2-diamine), studied by Lu et al.,[109] where L4 and MCP strictly resemble L3 in **Ni 11**, but acting as neutral ligands with only pyridyl branches. Their conformation leaves two *cis*-oriented sites capable of coordinating the water molecules. Both **Ni 12** and **Ni 13** undergo direct oxidation from Ni^{II} to Ni^{IV} during the catalytic cycle. They demonstrate moderate overpotentials of approximately 530 mV and 480 mV, respectively, in sodium acetate buffer at pH = 6.5. Mechanistic investigations reveal that the buffer anion plays a crucial role in the water oxidation process. Specifically, the presence of the base as a proton acceptor facilitates PCET, which reduces the barrier for O–O bond formation during the catalytic cycle.

Recent studies by Wang[110] leads to $[NiL5(H_2O)](ClO_4)_2$ **Ni 14** and $[NiL6(H_2O)](ClO_4)_2$ **Ni 15** (Figure 16, L5 = *N*1-benzyl-*N*1,*N*2,*N*2-tris(pyridin-2-ylmethyl)ethane-1,2-diamine, L6 = *N*1-benzyl-*N*1,*N*2,*N*2-tris(pyridin-2-ylmethyl)cyclohexane-1,2-diamine) featuring only one labile coordinated water molecule due to the employment of neutral nitrogen-donor pentadentate ligands. These complexes have shown interesting electrocatalytic water oxidation performances, with TOFs of 3.01 s^{-1} and 4.62 s^{-1}, respectively, similar overpotentials (~860 mV) and high stability and selectivity, with faradic efficiencies of 94–96 %.

Another flexible five-coordinate nickel catalyst [NiL7Cl](Cl) **Ni 16** (Figure 16, L7 = 2,6-bis(1,1-di(pyridin-2-yl)ethyl)pyridine) reported by Sun et al.,[111] demonstrates efficient water oxidation at a high rate of 145 s^{-1} at an overpotential of 800 mV, with stability across a wide pH range (7–10.8).

The trinuclear nickel complex $[Ni^{II}_3(ahp)(\mu\text{-}OH)_2](CF_3SO_3)_2$ **Ni 17** bearing the dianionic oligodentate aminohydroxopyridyl ligand ahp^{2-} (Figure 17) was recently reported by Zhang et al.[112] **Ni 17** acts as efficient MWOC and exhibits high catalytic performance and stability under neutral conditions (pH 7) with an overpotential of 340 mV and a TON of 13. Electrochemical studies disclosed cooperation among the three nickel sites in both charge accumulation and O–O bond formation. This catalyst could undergo $4e^-$ oxidation through involvement of all three nickel sites, and the O–O bond formation was triggered by a charge distribution process via PCET, also supported by DFT calculation.

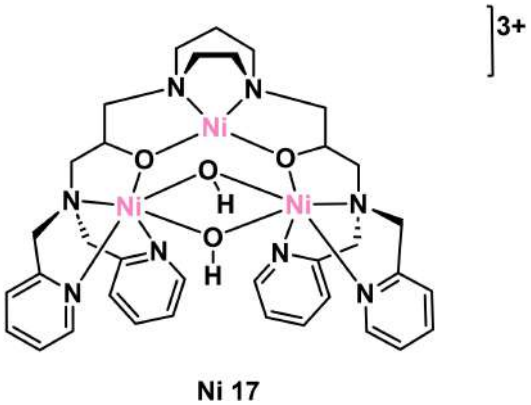

Ni 17

Figure 17. Molecular structure of $[Ni^{II}_3(ahp)(\mu\text{-}OH)_2](CF_3SO_3)_2$ **Ni 17**.

4.5. Iron Complexes for Electrocatalytic Water Oxidation

Iron complexes history as electrocatalysts for water oxidation start in 2014 with a work from Coggings and Meyer[113] who reported the first well-defined electrocatalytic iron based MWOC, an amidate-aqua Fe^{III} complex (**Fe 1** in Figure 18). The structure of this complex is based on the $[Fe^{III}(dpaq)(H_2O)]^{2+}$ species. This octahedral complex exhibited FE of 45%, an overpotential of 700 mV, and TOF of 0.15 s^{-1}. Notably, this complex showed good stability, with only minor decomposition observed under operating conditions, especially when compared to other iron-based WOCs that often decompose in acidic solutions driven by Ce^{IV} or $NaIO_4$ sacrificial oxidants. This complex, operating in propylene carbonate solution, achieves a substantial rate enhancement and undergoes a PCET mechanism to generate a $FeV(O)^{2+}$ intermediate. This intermediate reacts with water to form a peroxide species, which is then oxidized to generate molecular oxygen. The electrochemical mechanism for this complex has been characterized, and it operates through a water nucleophilic attack (WNA) mechanism, with the O−O bond formation serving as the rate determining step.

At first sight, the best single-site iron based electrocatalyst appeared to be the pentanuclear iron complexes **Fe 2–4** in Figure 18 reported by Masaoka and co-workers, which showed the highest TON and TOF of 10^7 and 1400 s^{-1}, respectively.[114] The CV of the complex showed that each Fe^{II}/Fe^{III} couple undergoes five reversible waves as sequentially occurring one-electron redox reactions. In 2019, the same authors also reported on the tunability of overpotential and TOF by ligand design.[115] Nevertheless, in 2020, Llobet and co-workers demonstrated iron oxide particles, formed due to complex decomposition, as the actual catalyst. Thus, **Fe 2–4** pentanuclear complexes are likely to decompose in quite active nanoparticles which, upon deposition on the electrode, are actually responsible for heterogeneous electrocatalysed water oxidation.[116] Discussion on stability and characterization of intermediates for pentanuclear iron complexes employed in

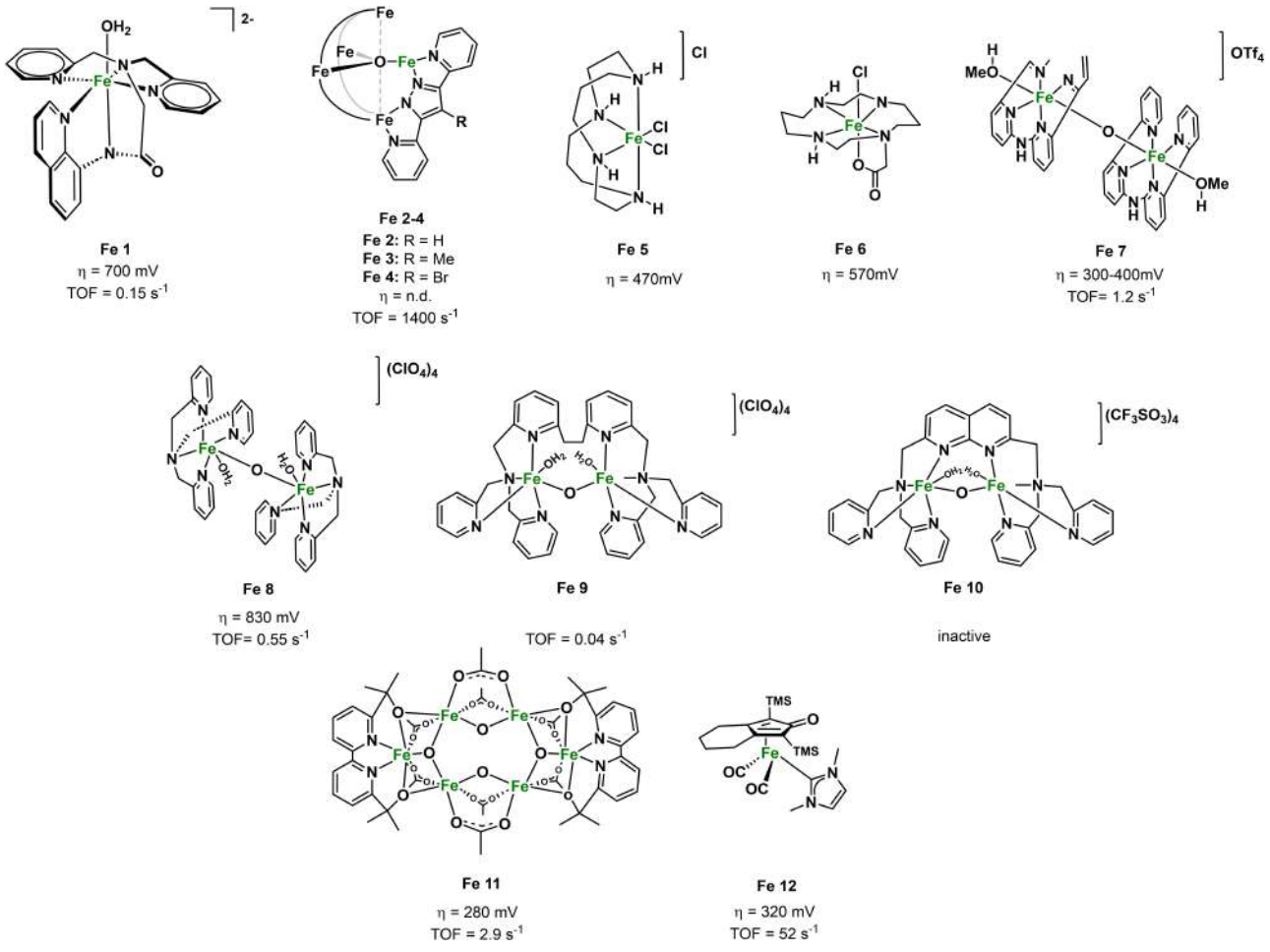

Figure 18. Iron complexes (**Fe 1–12**) for electrocatalytic water oxidation.

water oxidation has been recently re-opened by Puskar et al.,[117] exploiting *in situ* XAS, XANES and EPR studies to support a ligand role. The pentanuclear complexes have been also immobilized, in the same work, on MOF in order to move to photoelectro-catalytic application.

Hetterscheid explored in 2016 tetradentate ligands in **Fe 5** and **Fe 6** complexes (Figure 18) as another resource for electrocatalytic water oxidation[118] Interestingly, this water-soluble iron complex was evaluated using an online electrochemical mass spectrometry strategy. The **Fe 5** complex exhibited oxygen evolution at an onset potential of 1.7 V vs. NHE at pH 7.5, with an overpotential of 470 mV. This suggests that **Fe 5** operates through a cis-configuration, though its FE and TON were relatively low. Additionally, minor CO_2 formation was detected due to oxidative ligand decomposition, a common trait in iron-based molecular WOCs. In **Fe 6**, the introduction of an axially coordinating carboxylate group caused the onset potential to shift to 1.8 V vs. NHE, indicating that the carboxylate group plays a detrimental effect on the catalytic activity.

Further work from Hetterscheid et al.[119] based on the dinuclear **Fe 7** (Figure 18) catalyst in (0.1 M pH 7 Na_2SO_4 solution) with a carboxylate-bridged structure, showed interesting results. Using EQCM experiments, it was confirmed that the working electrode material significantly influences the electrocatalytic performance of **Fe 7**. Indeed, with pyrolytic graphite as the electrode, **Fe7** demonstrated a lower overpotential of 300–400 mV compared to 600 mV with a gold electrode. This suggests that the choice of electrode material plays a crucial role in the efficiency of the water oxidation process. These results were lately implemented in 2020 improving the whole efficiency acting a ligand design to dinuclear oxo-bridged iron MWOCs in organic solvents. NaOH was employed in this latter case as the source of oxygen.[120]

Structural regulation in the O–O bond formation, has also been more recently identified in dinuclear molecular iron water oxidation catalysts developed by the group of Zhang.[121] Complexes **Fe 8** and **Fe 9** (Figure 18) were found to be active as electrocatalysts for water oxidation (overpotential 830 mV, TOF: **Fe 8** 0.55 s^{-1}; **Fe 9** 0.04 s^{-1}) in 0.1 M $NaHCO_3$ solution (pH 8.4). On the other hand, more rigid complex **Fe 10** was found almost inactive. This behaviour is interestingly different from the similar **Cu 3** and **Cu 4** complexes (paragraph 4.3). O–O bond formation was achieved via intramolecular oxo/oxo or oxo/oxyl coupling and thus it required the spatial position match of the two Fe=O. DFT calculations suggested that the anti to syn isomerization of the two highvalent Fe=O moieties occur via the axial rotation of one Fe=O unit around the Fe-O–Fe center. This is followed by the O–O bond formation via an oxo–oxo coupling. Thus, the rigid BPMAN ligand in complex **Fe 10** limits the isomerization and axial rotation in agreement with the negligible catalytic activity. This work clarifies bimetallic cooperative effect, providing pathway for molecular design by metal and ligand rigidity regulation.

Same group also extended the scope of their research to **Fe-Ni** heterobimetallic synergistic effect in molecular water oxidation catalysis.[122] **Fe-Ni** complex reported in Figure 19, was tested in $NaHCO_3$ buffer with 10% CH_3CN (as cosolvent) using glassy carbon (GC) electrode. The catalytic rate constant was remarkable: 11.5 s^{-1} at pH 10.0 and 0.23 s^{-1} at pH 9.0.

Unless what found for **Fe-Ni** complex, which shows good activity and stability, monometallic dinuclear Fe–Fe and Ni–Ni complexes resulted unactive or highly unstable. The synergistic role of Fe and Ni was thus found by DFT calculation to promote O–O bond formation, with $Ni^{III}(\mu\text{-}O)Fe^{IV}=O$ as the key intermediate, followed by intramolecular oxyl-oxo coupling between bridged O radical and terminal $Fe^{IV}=O$ moiety. For further experimental and DFT calculation employed to follow the catalyst behaviour in water, to establish stability and intermediates formation as well as to have a deep insight into the recent discovery in dinuclear MWOC metal environment and structural regulation design, the reader is addressed to follow the highly detailed work of Zhang and co-workers.[80,120,121]

More recently an hexanuclear iron(III) water soluble complex (**Fe 11** in Figure 18) was investigated by Yu et al.[123] Complex **Fe 11** design was defined taking into account that a bipyalk ligand with strong electron-donating groups can improve the stability of high-oxidation-state intermediates formed during water oxidation. Complex **Fe 11** demonstrated stability and catalytic activity for water oxidation under acidic conditions, with TOF of 2.9 s^{-1}, and a low onset potential of 290 mV at pH 2, highlighting its efficiency as an electrocatalyst for water oxidation. DPV confirmed the presence of

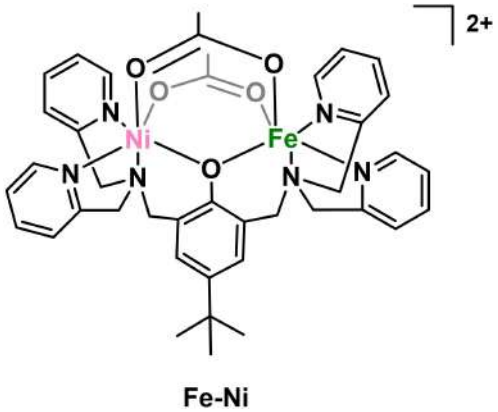

Fe-Ni

Figure 19. Heterobimetallic dinuclear **Fe-Ni** complex active as molecular water oxidation catalyst.

$Fe^{III}/^{IV}$ oxidation and mechanistic analysis suggested a PCET mechanism, which was consistent with the observed Nernstian slope of −57 mV per pH unit.

Our group has been working for years in the development of molecular redox catalysts bearing cyclopentadienone and N-heterocyclic carbene (NHC) ligands. These peculiar ligands combination allow cyclopentadienone to be employed as a non-innocent ligand in bifunctional catalysis, on the other hand, the ancillary NHC donor ligand further allow the tuning of electrochemical behaviour.[124] Taking also advantage from the group experience in dinuclear iron hydrogenase mimic complexes previously developed,[125] and despite the low valency of the iron center in **Fe 12**, this complex has been found electroactive in water oxidation at basic pH with a good overpotential.[32] A family of differently substituted NHC complex of **Fe 12** type have been screened, indicating a role for both cyclopentadienone and NHC in the electrocatalytic behaviour. Nevertheless, an electrowithdrawing group on the cyclopentadienone ligand lowered the reaction efficiency and redox reactive substituents on NHC (such as $-NH_2$) influenced the reaction, revealing **Fe 12** as the best catalyst of this family (water/THF mixture, basic conditions) with an interesting overpotential of 320 mV and TOF = 52 s^{-1}. Reactivity studies, together with EPR characterization and DFT calculations demonstrated the stability of the complex under catalytic conditions, confirmed the role of NHC in tuning the complex potential, and identified cyclopentadienone as a non-innocent ligand able to stabilize a persistent radical complex after a monoelectronic oxidation (Figure 20). This peculiar ligand combination has been employed for the first time in electrocatalytic MWOC reaction, further investigations are thus required in order to shed light on the mechanism and to exploit the system to improve first row MWOC efficiency.

Attempts to graft the molecular reactivity onto insoluble substrates through immobilization of iron complexes could be exploited in order to put together the advantages of molecular catalysis and heterogeneous systems,[126] both in the case of unreactive supports or designing hybrid systems in which the molecule and the insoluble substrate have both an electrocatalytic effect. This field is still in its infancy for iron MWOC if compared with the exiting results obtained by the group of Llobet with copper complexes (see paragraph 4.3). At the moment only two examples are reported on ITO iron MWOC immobilization.[127] However, both cases suffered from catalyst decomposition to iron oxide during catalytic cycles,[128] avoiding exploiting the molecular structures advantages.

5. Summary and Outlook

Synthetic water splitting is widely recognized as a promising Nature-inspired approach for producing sustainable energy through green electrolysis. Within this framework, catalysis, and particularly electrocatalysis, plays a crucial role in developing new strategies. Active and stable electrocatalysts, especially for the more energy demanding water oxidation, represent a way of exploration that engage researchers with increasing interest. From one side, heterogeneous electrocatalysis usually performs water oxidation with low overpotential and high stability. On the other hand, it requires high (often noble) metal loadings and a peculiar control of the morphology to ensure optimal surface area and accessibility of catalytic sites. On the homogeneous side, MWOCs face challenges such as higher working overpotential and lower stability compared to the heterogeneous counterparts. However, from a more positive perspective, MWOCs work with well-defined catalytic sites, a much better atom economy, and they often show higher efficiency. Thanks to their intrinsic modularity, suitable ligands enable fine tuning of electrochemical properties, as well as the possibility to be decorated with functionalization that allows immobilization on inert or non-innocent supports (such as in hybrid materials). Furthermore, the reaction conditions could improve both energetic costs and overall selectivity. Nevertheless, tuning MWOCs to finely control several parameters is deeper due to the directional previsions on inner and outer sphere cooperation by means of mechanistic investigations. In the present manuscript a rapid excursus on heterogeneous catalysis is introduced to

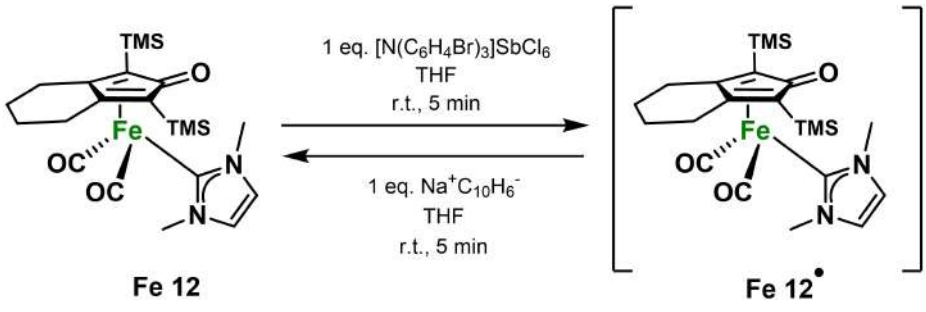

Figure 20. Reversible generation of the radical complex **Fe 12**.

have in hands the numbers to be compared with MWOCs. A discussion on the similarities and differences between heterogeneous and homogeneous systems has been provided as an additional framework for effective comparison. The exceptional efficiency achieved with ruthenium complexes, still the best-performing catalysts in molecular electrocatalytic water oxidation, serves as a benchmark for evaluating the thresholds that first-row transition metal-based MWOCs must reach and surpass. Several mono- and multi-dentate ligands have been employed with different earth abundant metals, namely Mn, Co, Cu, Ni and Fe in different oxidation states. The plethora of examples reported explores the theme in several ways: design of the ligands, by changing steric and electronic properties through electron donor or electron withdrawing substituents. Monitoring reaction upon pH variation, when the reaction or the ligand appeared to be pH dependent, gave back important information on overpotential and efficiency behaviours. Several characterizations, ranging from NMR, IR, EPR, Raman, UV-vis measurements (also *in situ)*, EQCM experiments, chronoamperometry, X-ray photoelectron spectroscopy to cite a few, are now available to deeply understand the destiny and the stability of the molecular electrocatalysts. Among the most exciting recent advances is the work of Llobet's group, pioneers in the field, who have reported the first example of a first-row transition metal-based MWOC anchored to a conductive solid support (exploiting electropolymerization of a thiophene-functionalized copper complex) developing a hybrid material able to work under neutral pH. This hybrid catalyst maintains its integrity after more than 11,000 TONs. Such developments pave the way for the integration of earth-abundant MWOCs into photoelectrochemical devices.

Abbreviations

WOC	Water Oxidation Catalyst
MWOC	Molecular Water Oxidation Catalyst
OER	Oxygen Evolution Reaction
CNTs	Carbon Nanotubes
TON	Turnover Number
TOF	Turnover Frequency
FE	Faradaic Efficiency
OEC	Oxygen-Evolving Complex
PSII	photosystem II
TPP	triphenylporphyrin
XPS	X-ray Photoelectron Spectroscopy
SCE	Saturated Calomel Electrode
NHE	Normal Hydrogen Electrode
DFT	Density Functional Theory
PCET	Proton-Coupled Electron Transfer
TDMImP	5,10,15,20-tetrakis-(1,3-dimethylimidazolium-2-yl) porphyrin
TAML	tetraamido(4−) macrocyclic ligands
CV	Cyclic voltammetry
EQCM	Electrochemical Quartz Crystal Microbalance
EDTA	ethylenediaminetetraacetic acid
CPE	Controlled Potential Electrolysis
DPV	Differential Pulse Voltammetry
SEM	Scanning Electron Microscopy
TGG	triglycylglycine
pimH	2-(2'-pyridyl)-imidazole
ITO	Indium Tin Oxide
GC/CNT	Glassy Carbon/Carbon NanoTubes
XAS	X-ray Absorption Spectroscopy
PEC	PhotoElectroChemical
WNA	Water Nucleophilic Attack
XANES	X-ray Absorption Near Edge Structure
MOF	MetalOrganic Framework
NHC	N-Heterocyclic carbene

Acknowledgements

We gratefully acknowledge the University of Bologna. Open Access publishing facilitated by Università degli Studi di Bologna, as part of the Wiley - CRUI-CARE agreement.

References

[1] a) N. S. Lewis, D. G. Nocera, *Proc. Natl. Acad. Sci. U. S. A.* **2006**, *103*, 15729–15735; b) D. G. Nocera, *Inorg. Chem.* **2009**, *48*, 10001–10017; c) D. Gust, T. A. Moore, A. L. Moore, *Acc. Chem. Res.* **2009**, *42*, 1890–1898; d) S. Berardi, S. Drouet, L. Francàs, C. Gimbert-Suriñach, M. Guttentag, C. Richmond, T. Stoll, A. Llobet, *Chem. Soc. Rev.* **2014**, *43*, 7501–7519; e) J. Barber, *Chem. Soc. Rev.* **2009**, *38*, 185–196; f) D. G. Nocera, *Acc. Chem. Res.* **2012**, *45*, 767–776.

[2] a) W. R. Stahel, *Nature* **2016**, *531*, 435–438; b) A. C. Dillon, K. M. Jones, T. A. Bekkedahl, C. H. Kiang, D. S. Bethune, M. J. Heben, *Nature* **1997**, *386*, 377–379; c) E. Tsivion, J. R. Long, M. Head-Gordon, *J. Am. Chem. Soc.* **2014**, *136*, 17827–17835; d) L. Roy, S. Mittal, A. Paul, *Angew. Chem., Int. Ed.* **2012**, *51*, 4152–4156; e) L. Roy, S. Bhunya, A. A. Paul, *Angew. Chem., Int. Ed.* **2014**, *53*, 12430–12435; f) L. Roy, A. Paul, *Chem. Commun.* **2015**, *51*, 10532–10535; g) L. Roy, *Int. J. Quantum Chem.* **2020**, *120*, No. e26257; h) P. Agarwala, S. K. Pati, L. Roy, *Mol. Phys.* **2020**, *118*, No. e1757169.

[3] a) A. Bard, M. A. Fox, *Acc. Chem. Res.* **1995**, *28*, 141–145; b) T. J. Meyer, *Acc. Chem. Res.* **1989**, *22*, 163–170; c) M. Yagi, M. Kaneko, *Chem. Rev.* **2001**, *101*, 21–36; d) J. D. Blakemore, R. H. Crabtree, G. W. Brudvig, *Chem. Rev.* **2015**, *115*, 12974–13005.

[4] a) S. Liu, Y. Wei, M. Wang, Y. Shen, *Coord. Chem. Rev.* **2025**, *522*, 216190; b) R. Sen, S. Das, A. Nath, P. Maharana,

P. Kar, F. Verpoort, P. Liang, S. Roy, *Front. Chem.* **2022**, *10*, 861604; c) P. Li, R. Zhao, H. Chen, H. Wang, P. Wei, H. Huang, Q. Liu, T. Li, X. Shi, Y. Zhang, M. Liu, X. Sun, *Small* **2019**, *15*, 1805103.

[5] See for some example of Ru- and Ir-based electrocatalysts: a) A. L. Strickler, R. A. Flores, L. A. King, J. K. Nørskov, M. Bajdich, T. F. Jaramillo, *ACS Appl. Mater. Inter.* **2019**, *11*, 34059–34066; b) M. A. Hubert, A. M. Patel, A. Gallo, Y. Liu, E. Valle, M. Ben-Naim, J. Sanchez, D. Sokaras, R. Sinclair, J. K. Nørskov, L. A. King, M. Bajdich, T. F. Jaramillo, *ACS Catal.* **2020**, *10*, 12182–12196.

[6] a) A. S. Jamadar, J.B Yadav, Metal Oxide-Based Electrocatalytic Materials. In: Patra, S., Shukla, S. K., Sillanpää, M. (eds) Electrocatalytic Materials. Springer, Cham. **2024**. b) A. S. Jamadar, R. Sutar, S. Patil, R. Khandekar, J. B. Yadav, *Materials Reports: Energy* **2024**, *4*, 100283.

[7] B. M. Hunter, H. B. Gray, H. B. Müller, *Chem. Rev.* **2016**, *116*, 14120–14136.

[8] A. Chatterjee, P. Chakraborty, B. Kumar, S. Mandal, S. K. Dey, *ChemCatChem* **2024**, *16*, e202400622.

[9] L. Han, X.-Y. Yu, X. W. D. Lou, *Adv. Mater.* **2016**, *28*, 4601–4605.

[10] M. Gorlin, P. Chernev, J. Ferreira de Araújo, T. Reier, S. R. Dresp, B. Paul, R. Krahnert, H. Dau, P. Strasser, *J. Am. Chem. Soc.* **2016**, *138*, 5603–5614.

[11] N. Chen, J. Qi, X. Du, Y. Wang, W. Zhang, Y. Wang, Y. Lu, S. Wang, *RSC Adv.* **2016**, *6*, 103541–103545.

[12] D. Tonelli, I. Gualandi, E. Musella, E. Scavetta, *Nanomaterials* **2021**, *11*, 725.

[13] R. Subbaraman, D. Tripkovic, K.-C. Chang, D. Strmcnik, A. P. Paulikas, P. Hirunsit, M. Chan, J. Greeley, V. Stamenkovic, N. M. Markovic, *Nat. Mater.* **2012**, *11*, 550–557.

[14] E. Musella, I. Gualandi, E. Scavetta, M. Gazzano, A. Rivalta, E. Venuti, M. Christian, V. Morandi, D. Tonelli, *Chem. Eur. J.* **2019**, *25*, 16301–16310.

[15] I. Gualandi, E. Musella, G. Costa, M. Gazzano, E. Scavetta, S. Zappoli, D. Tonelli, *Adv. Energy Sustainability Res.* **2024**, 2400233.

[16] a) Y. Zhu, W. Zhou, J. Sunarso, Y. Zhong, Z. Shao, *Adv. Funct. Mater.* **2016**, *26*, 5862–5872; b) F. Song, K. Schenk, X. Hu, *Energ. Environ. Sci.* **2016**, *9*, 473–477; c) J. Suntivich, K. J. May, H. A. Gasteiger, J. B. Goodenough, Y. Shao-Horn, *Science* **2011**, *334*, 1383–1385.

[17] S. Ghosh, S. Bera, S. Samajdar, S. Pal, *WIREs Energy and Environment* **2023**, *12*, e458.

[18] a) S. Chen, J. Duan, M. Jaroniec, S.-Z. Qiao, *Adv. Mater.* **2014**, *26*, 2925–2930; b) X. Yu, M. Zhang, J. Chen, Y. Li, G. Shi, *Adv. Energ. Mater.* **2016**, *6*, 1501492.

[19] Y. P. Zhu, C. Guo, Y. Zheng, S.-Z. Qiao, *Acc. Chem. Res.* **2017**, *50*, 915–923.

[20] M. Tahir, N. Mahmood, L. Pan, Z.-F. Huang, Z. Lv, J. Zhang, F. K. Butt, G. Shen, X. Zhang, S. X. Douc, J.-J. Zou, *J. Mater. Chem. A.* **2016**, *4*, 12940–12946.

[21] B. Wang, C. Tang, H.-F. Wang, X. Chen, R. Cao, Q. Zhang, *J. Energ. Chem.* **2019**, *38*, 8–14.

[22] A. K. Singh, L. Roy, *ACS Omega* **2024**, *9*, 9886–9920.

[23] P. T. Smith, E. M. Nichols, Z. Cao, C. J. Chang, *Acc. Chem. Res.* **2020**, *53*, 575–587.

[24] a) N. Vereshchuk, M. Gil-Sepulcre, A. Ghaderian, J. Holub, C. Gimbert-Surinach, A. Llobet, *Chem. Soc. Rev.* **2023**, *52*, 196–211; b) H.-C. Ma, S.-C. Hsiao, Y.-H. Wang, *Catal. Sci. Technol.* **2023**, *13*, 1598–1622; c) H. Dau, C. Limberg, T. Reier, M. Risch, S. Roggan, P. Strasser, *ChemCatChem* **2010**, *2*, 724–761.

[25] a) M. A. Khan, S. Khan, S. Sengupta, B. N. Mongal, S. Naskar, *Coord. Chem. Rev.* **2024**, *504*, 215679; b) M. Raj, S. K. Padhi, *Chem. Rec.* **2024**, e202400170; c) A. R. Parent, K. Sakai, *ChemSusChem* **2014**, *7*, 2070–2080; d) M. Sutradhar, A. J. L. Pombeiro, J. A. L. da Silva, *Coord. Chem. Rev.* **2021**, *439*, 213911; e) L.-H. Zhang, S. Mathew, J. Hessels, J. N. H. Reek, F. Yu, *ChemSusChem* **2021**, *14*, 234–250; f) S. Fukuzumi, D. Hong, *Eur. J. Inorg. Chem.* **2014**, 645–659.

[26] a) A. Vazhayil, L. Vazhayal, J. Thomas, S. Ashok, N. Thomas, *Appl. Surf. Sci. Adv.* **2021**, *6*, 100184; b) M. Tahir, L. Pana, F. Idrees, X. Zhang, L. Wang, J. Zou, Z. L. Wang, *Nano Energy* **2017**, *37*, 136–157.

[27] C. C. L. McCrory, S. Jung, I. M. Ferrer, S. M. Chatman, J. C. Peters, T. F. Jaramillo, *J. Am. Chem. Soc.* **2015**, *137*, 4347–4357.

[28] D. Lebedev, R. Ezhov, J. Heras-Domingo, A. Comas-Vives, N. Kaeffer, M. Willinger, X. Solans-Monfort, X. Huang, Y. Pushkar, C. Copéret, *ACS Cent. Sci.* **2020**, *6*, 1189–1198.

[29] Y. Wang, Z. Xu, X. Wu, Z.-S. Wu, *Green En. Env.* **2024**, *9*, 1497–1517.

[30] R. Ezhov, A. Karbakhsh Ravari, Y. Pushkar, *Angew. Chem., Int. Ed.* **2020**, *59*, 13502–13505.

[31] X. Zhang, Q.-F. Chen, J. Deng, X. Xu, J. Zhan, H.-Y. Du, Z. Yu, M. Li, M.-T. Zhang, Y. Shao, *J. Am. Chem. Soc.* **2022**, *144*, 17748–17752.

[32] A. J. R. Botz, M. Nebel, R. A. Rinc'on, E. Ventosa, W. Schuhmann, *Electrochim. Acta* **2015**, *179*, 38–44.

[33] L. Han, S. Dong, E. Wang, *Adv. Mater.* **2016**, *28*, 9266–9291.

[34] K. Fominykh, J. M. Feckl, J. Sicklinger, M. Döblinger, S. Böcklein, J. Ziegler, L. Peter, J. Rathousky, E. Scheidt, T. Bein, D. Fattakhova-Rohlfing, *Adv. Funct. Mater.* **2014**, *24*, 3123–3129.

[35] a) T. Zhang, C. Wang, S. Liu, J. Wang, W. Lin, *J. Am. Chem. Soc.* **2014**, *136*, 273–281; b) Y. Tamaki, A. K. Vannucci, C. J. Dares, R. A. Binstead, T. J. Meyer, *J. Am. Chem. Soc.* **2014**, *136*, 6854–6857; c) S. M. Barnett, K. I. Goldberg, J. M. Mayer, *Nat. Chem.* **2012**, *4*, 498–502.

[36] a) A. Cingolani, I. Gualandi, E. Scavetta, C. Cesari, S. Zacchini, D. Tonelli, V. Zanotti, P. Franchi, M. Lucarini, E. Sicilia, G. Mazzone, D. Nanni, R. Mazzoni, *Catal. Sci. Technol.* **2021**, *11*, 1407–1417; b) L. Duan, L. Wang, A. K. Inge, A. Fischer, X. Zou, L. Sun, *Inorg. Chem.* **2013**, *52*, 7844–7852.

[37] C. Costentin, S. Drouet, M. Robert, J.-M. Savéant, *J. Am. Chem. Soc.* **2012**, *134*, 11235–11242.

[38] S. W. Gersten, G. J. Samuels, T. J. Meyer, *J. Am. Chem. Soc.* **1982**, *104*, 4029–4030.

[39] a) H. W. Tseng, R. Zong, J. T. Muckerman, R. Thummel, *Inorg. Chem.* **2008**, *47*, 11763–11773; b) J. J. Concepcion, J. W. Jurss, J. L. Templeton, T. J. Meyer, *J. Am. Chem. Soc.* **2008**, *130*, 16462–16463; c) S. Masaoka, K. Sakai, *Chem. Lett.* **2009**, *38*, 182–183; d) D. J. Wasylenko, C. Ganesamoorthy, B. D. Koivisto, M. A. Henderson, C. P. Berlinguette, *Inorg. Chem.* **2010**, *49*, 2202–2209.
[40] H.-C. Ma, S.-C. Hsiao, Y.-H. Wang *Catal. Sci. Technol.* **2023**, *13*, 1598–1622.
[41] B. J. J. Timmer, O. Kravchenko, B. Zhang, T. Liu, L. Sun, *Inorg. Chem.* **2021**, *60* 1202–1207.
[42] Y. Xu, A. Fischer, L. Duan, L. Tong, E. Gabrielsson, B. Akermark, L. Sun, *Angew. Chem., Int. Ed.* **2010**, *49*, 8934–8937.
[43] B. J. J. Timmer, O. Kravchenko, B. Zhang, T. Liu, L. Sun, *Inorg. Chem.* **2021**, *60*, 1202–1207.
[44] R. Matheu, M. Z. Ertem, J. Benet-Buchholz, E. Coronado, V. S. Batista, X. Sala, A. Llobet, *J. Am. Chem. Soc.* **2015**, *137*, 10786–10795.
[45] N. Vereshchuk, R. Matheu, J. Benet-Buchholz, M. Pipelier, J. Lebreton, D. Dubreuil, A. Tessier, C. Gimbert-Suriñach, M. Z. Ertem, A. Llobet, *J. Am. Chem. Soc.* **2020**, *142*, 5068–5077.
[46] D. Scherrer, M. Schilling, S. Luber, T. Fox, B. Spingler, R. Alberto, C. J. Richmond, *Dalton Trans.* **2016**, *45*, 19361–19367.
[47] M. A. Hoque, M.s Gil-Sepulcre, A. de Aguirre, J. A. A. W. Elemans, D. Moonshiram, R. Matheu, Y. Shi, J. Benet-Buchholz, X. Sala, M. Malfois, E. Solano, J. Lim, A. Garzón-Manjón, C. Scheu, M. Lanza, F. Maseras, C. Gimbert-Surinach, A. Llobet, *Nature Chem.* **2020**, *12*, 1060–1066.
[48] M. Salati, F. Dorchies, J.-W. Wang, M. Ventosa, S. González-Carrero, C. Bozal-Ginesta, J. Holub, O. Rudiger, S. DeBeer, C. Gimbert-Surinach, J. R. Durrant, M. Z. Ertem, M. Gil-Sepulcre, A. Llobet, *Small* **2024**, 2406375.
[49] J. Patel, G. Bury, Y. Pushkar, *Small* **2024**, *20*, 2310106.
[50] a) J. Shi, Y.-H. Guo, Q.-F. Chen, M.-T. Zhang, *Angew. Chem. Int. Ed.* **2020**, *59*, 4000–4008; b) J. Shi, Y.-H. Guo, F. Xie, M.-T. Zhang, H.-T. Zhang, *Chinese J. Catal.* **2023**, *52*, 271; c) Q.-F. Chen, X. Zhang, J. Shi, J. Zhan, F. Xie, H.-T. Zhang, J. Deng, J. Liu, M. Li, Y. Shao, M.-T. Zhang, *CCS Chem.* **2024**, DOI: 10.31635/ccschem.024.202403935.
[51] M. Okamura, S. Masaoka, *Chem. Asian J.* **2015**, *10*, 306–315.
[52] C. Zhang, C. Chen, H. Dong, J. R. Shen, H. Dau, J. Zhao, *Science* **2015**, *348*, 690–693.
[53] K. Wieghardt, U. Bossek, W. Gebert, *Angew. Chem., Int. Ed. Engl.* **1983**, *22*, 328–329.
[54] C. E. Dube, S. Mukhopadhyay, P. J. Jr Bonitatebus, R. J. Staples, W.-H. Armstrong, *Inorg. Chem.* **2005**, *44*, 5161–5175.
[55] W. F. Ruettinger, C. Campana, G. C. Dismukes, *J. Am. Chem. Soc.* **1997**, *119*, 6670–6671.
[56] J. B. Vincent, C. Christmas, J. C. Huffman, G. Christou, H. .-R. Chang, D. N. Hendrickson, *J. Chem. Soc. Chem. Commun.* **1987**, *4*, 236–238.
[57] J. S. Kanady, E. Y. Tsui, M. W. Day, T. A. Agapie, *Science* **2011**, *333*, 733–736.
[58] Y. Naruta, M. Sasayama, T. Sasaki, *Angew. Chem. Int. Ed. Engl.* **1994**, *33*, 1839–1841.
[59] a) T. Privalov, L. Sun, B. Akermark, J. Liu, Y. Gao, M. Wang, *Inorg. Chem.* **2007**, *46*, 7075–7086; b) Y. Gao, T. Akermark, J. Liu, L. Sun, B. Akermark, *J. Am. Chem. Soc.* **2009**, *131*, 8726–8727.
[60] a) P. Kurz, G. Berggren, M. F. Anderlund, S. Styring, *Dalton Trans.* **2007**, 4258–4261; b) K. Beckmann, H. Uchtenhagen, G. Berggren, M. F. Anderlund, A. Thapper, J. Messinger, S. Styring, P. Kurz, *Energy Environ. Sci.* **2008**, *1*, 668–676.
[61] M. Raj, S. K. Padhi, *Eur. J. Inorg. Chem.* **2022**, e202200238.
[62] G. Maayan, N. Gluz, G. A. Christou, *Nat. Catal.* **2018**, *1*, 48–54.
[63] a) Y. Y. Li, K. Ye, P. M. E. Siegbahn, R. Z. Liao, *ChemSusChem.* **2017**, *10*, 903–911.
[64] S. Zheng, X. Liang, C. Dai, X. Yang, Z. Li, Y. Lai, L. Honga, J. Lin, *New J. Chem.* **2023**, *47*, 13979–13984.
[65] N. S. McCool, D. M. Robinson, J. E. Sheats, G. Dismukes, *J. Am. Chem. Soc.* **2011**, *133*, 11446–11449.
[66] R. G. Hadt, D. Hayes, C. N. Brodsky, A. M. Ullman, D. M. Casa, M. H. Upton, D. G. Nocera, L. X. Chen, *J. Am. Chem. Soc.* **2016**, *138*, 11017–11030.
[67] R. Ezhov, A. Karbakhsh Ravari, G. Bury, P. F. Smith, Y. Pushkar, *Chem. Catal.* **2021**, *1*, 407–422.
[68] a) S. Fukuzumi, S. Mandal, K. Mase, K. Ohkubo, H. Park, J. Benet-Buchholz, W. Nam, A. Llobet, *J. Am. Chem. Soc.* **2012**, *134*, 9906–9909; b) M. L. Rigsby, S. Mandal, W. Nam, L. C. Spencer, A. Llobet, S. S. Stahl, *Chem. Sci.* **2012**,*3*, 3058–3062.
[69] D. K. Dogutan, R. McGuire, D. G. Nocera, *J. Am. Chem. Soc.* **2011**, *133*, 9178–9180.
[70] H. Sun, Y. Han, H. Lei, M. Chen, R. Cao, *Chem. Commun.* **2017**, *53*, 6195–6198.
[71] D. J. Wasylenko, C. Ganesamoorthy, J. Borau-Garcia, C. P. Berlinguette, *Chem. Commun.* **2011**, *47*, 4249–4251.
[72] D. Das, S. Pattanayak, K. Singh, B. Garai, S. S. Sayam, *Chem. Commun.* **2016**, *52*, 11787–11790.
[73] D. Wang, J. T. Groves, *Proc. Natl. Acad. Sci. USA* **2013**, *110*, 15579–15584.
[74] H.-Y. Du, S.-C. Chen, X.-J. Su, L. Jiao, M.-T. Zhang, *J. Am. Chem. Soc.* **2018**, *140*, 1557–1565.
[75] D. den Boer, Q. Siberie, M. A. Siegler, T. H. Ferber, D. C. Moritz, J. P. Hofmann, D. G. H. Hetterscheid, *ACS Catal.* **2022**, *12*, 4597–4607.
[76] M. W. Kanan, J. Yano, Y. Surendranath, M. Dincă, V. K. Yachandra, D. G. Nocera, *J. Am. Chem. Soc.* **2010**, *132*, 13692–13701.
[77] Y. Chen, X. Meng, X. Chen, X. Li, H. Ye, S. Liu, Z. Ruan, X. Liang, J. Lin, *Sustain Ener Fuels* **2023**,*7*, 242–247.
[78] X. Zhang, Y. Y. Li, J. Jiang, R. Zhang, R. Z. Liao, M. Wang, *Inorg.Chem.* **2020**, *59*, 5424–5432.
[79] X.-J. Su, M. Gao, L. Jiao, R.-Z. Liao, P. E. M. Siegbahn, J.-P. Cheng, M.-T. Zhang, *Angew. Chem. Int. Ed.* **2015**, *54*, 4909–4914; *Angew. Chem.* **2015**, *127*, 4991–4996.
[80] Q.-F. Chen, K.-L. Xian, H.-T. Zhang, X.-J. Su, R.-Z. Liao, M.-T. Zhang, *Angew. Chem. Int. Ed.* **2024**, *63*, e202317514.

[81] S. M. Barnett, K. I. Goldberg, J. M. Mayer, *Nat. Chem.* **2012**, *4*, 498–502.

[82] a) D. Y. Shopov, B. Rudshteyn, J. Campos, V. S. Batista, R. H. Crabtree, G. W. Brudvig, *J. Am. Chem. Soc.* **2015**, *137*, 7243–7250; b) S. B. Sinha, D. Y. Shopov, L. S. Sharninghausen, D. J. Vinyard, B. Q. Mercado, G. W. Brudvig, R. H. Crabtree, *J. Am. Chem. Soc.* **2015**, *137*, 15692–15695.

[83] L. A. Stott, K. E. Prosser, E. K. Berdichevsky, C. J. Walsby, J. J. Warren, *Chem. Commun.* **2017**, *53*, 651–654.

[84] T. Ghosh, P. Ghosh, M. A. Maayan, *ACS Catal.* **2018**, *8*, 10631–10640.

[85] M.-C. Kafentzi, R. Papadakis, F. Gennarini, A. Kochem, O. Iranzo, Y. Le Mest, N. Le Poul, T. Tron, B. Faure, A. J. Simaan, M. Reglier, *Chem. Eur. J.* **2018**, *24*, 5213–5224.

[86] M. K. Coggins, M. T. Zhang, Z. Chen, N. Song, T. J. Meyer, *Angew. Chem. Int. Ed.* **2014**, *53*, 12226–12230.

[87] M. T. Zhang, Z. Chen, P. Kang, T. J. Meyer, *J. Am. Chem. Soc.* **2013**, *135*, 2048–2051.

[88] P. Garrido-Barros, I. Funes-Ardoiz, S. Drouet, J. Benet-Buchholz, F. Maseras, A. Llobet, *J. Am. Chem. Soc.* **2015**, *137*, 6758–6761.

[89] P. Garrido-Barros, C. Gimbert-Surinach, D. Moonshiram, A. Picon, P. Monge, V. S. Batista, A. Llobet, *J. Am. Chem. Soc.* **2017**, *139*, 12907–12910.

[90] S. Chattopadhyay, A. Ghatak, Y. Ro, R. Guillot, Z. Halime, A. Aukauloo, A. Dey, *Inorg. Chem.* **2021**, *60*, 9442–9455.

[91] a) J. S. Pap, L. Szyrwiel, D. Sranko, Z. Kerner, B. Setner, Z. Szewczuk, W. Malinka, *Chem. Commun.* **2015**, *51*, 6322–6324; b) J. S. Pap, L. Szyrwiel, D. Sranko, Z. Kerner, B. Setner, Z. Szewczuk, W. Malinka, *Chem. Commun.* **2015**, *51*, 6322–6324.

[92] F. Yu, F. Li, J. Hu, L. Bai, Y. Zhu, L. Sun, *Chem. Commun.* **2016**, *52*, 10377–10380.

[93] Y. Liu, Y. Han, Z. Zhang, W. Zhang, W. Lai, Y. Wang, R. Cao, *Chem. Sci.* **2019**, *10*, 2613–2622.

[94] D. D. Boer, A. I. Konovalov, A. S. Maxime, D. G. H. Hetterscheid, *Inorg. Chem.* **2023**, *62*, 5303–5314.

[95] S. Khan, S. Sengupta, M. d Adnan Khan, M. P. Sk, N. C. Jana, S. Naskar, *Inorg. Chem.* **2024**, *63*, 1888–1897.

[96] M. Gil-Sepulcre, P. Pelosin, P. Garrido-Barros, J. Benet-Buchholz, A. Llobet, *ACS Appl. Energy Mater.* **2024**, *7*, 2561–2569.

[97] S. Amthor, K. Ranu, C. G. Bellido, F. F. Salomón, A. Piccioni, R. Mazzaro, F. Boscherini, L. Pasquini, M. Gil-Sepulcre, A. Llobet, *Adv. Mater.* **2024**, *36*, 2308392.

[98] Q.-F. Chen, Z.-Y. Cheng, R.-Z. Liao, M.-T. Zhang, *J. Am. Chem. Soc.* **2021**, *143*, 19761–19768.

[99] W. Shin, U. M. Sundaram, J. L. Cole, H. H. Zhang, B. Hedman, K. O. Hodgson, E. I. Solomon, *J. Am. Chem. Soc.* **1996**, *118*, 3202–3215.

[100] M. Zhang, M.-T. Zhang, C. Hou, Z.-F. Ke, T.-B. Lu, *Angew. Chem. Int. Ed.* **2014**, *53*, 13042–13048; *Angew. Chem.* **2014**, *126*, 13258–13264.

[101] J.-W. Wang, C. Hou, H.-H. Huang, W.-J. Liu, Z.-F. Ke, T.-B. Lu, *Catal. Sci. Technol.* **2017**, *7*, 5585–5593.

[102] L.-H. Zhang, F. Yu, Y. Shi, F. Li, H. Li, *Chem. Commun.* **2019**, *55*, 6122–6125.

[103] B. Ariela, W. Yaniv, S. Dror, K. Haya, A. Yael, M. Ericb, M. Dan, *Dalton Trans.* **2017**, *46*, 10774–10779.

[104] Y. Han, Y. Wu, W. Lai, R. Cao, *Inorg. Chem.* **2015**, *54*, 5604–5613.

[105] J. W. Wang, X. Q. Zhang, H. H. Huang, T. B. Lu, *ChemCatChem.* **2016**, *8*, 3287–3293.

[106] J. Lin, P. Kang, X. Liang, B. Ma, Y. Ding, E *lectrochim. Acta* **2017**, *258*, 353–359.

[107] H. Lee, X. Wu, L. Sun, *ChemSusChem* **2020**, *13*, 3277–3282.

[108] D. Wang, C. O. Bruner, *Inorg. Chem.* **2017**, *56*, 13638–13641.

[109] [1] a) G.-Y. Luo, H.-H. Huang, J.-W. Wang, T.-B. Lu, *ChemSusChem* **2016**, *9*, 485–491; b) J.-W. Wang, X.-Q. Zhang, H.-H. Huang, T.-B. Lu, *ChemCatChem* **2016**, *8*, 3287–3293.

[110] J. Shen, M. Wang, T. He, J. Jiang, M. Hu, *Chem. Commun.* **2018**, *54*, 9019–9022.

[111] L. Wang, L. Duan, R. B. Ambre, Q. Daniel, H. Chen, J. Sun, B. Das, A. Thapper, J. Uhlig, P. Diner, L. Sun, *J. Catal.* **2016**, *335*, 72–78.

[112] Q.-F. Chen, Y. Xiao, R.-Z. Liao, M.-T. Zhang, *CCS Chem.* **2023**, *5*, 245–256, DOI: 10.31635/ccschem.022.202101668.

[113] M. K. Coggins, M. T. Zhang, A. K. Vannucci, C. J. Dares, T. J. Meyer, *J. Am. Chem. Soc.* **2014**, *136*, 5531–5534.

[114] M. Okamura, M. Kondo, R. Kuga, Y. Kurashige, T. Yanai, S. Hayami, V. K. Praneeth, M. Yoshida, K. Yoneda, S. Kawata, S. Masaoka, *Nature* **2016**, *530*, 465–468.

[115] V. K. K. Praneeth, M. Kondo, M. Okamura, T. Akai, H. Izu, S. Masaoka, *Chem. Sci.* **2019**, *10*, 4628–4639.

[116] Pelosin, M. Gil-Sepulcre, P. Garrido-Barros, D. Moonshiram, J. Benet-Buchholz, C. Gimbert-Surinach, A. Llobet, *iScience* **2020**, *23*, 101378.

[117] R. Ezhov, G. Bury, O. Maximova, E. D. Grant, M. Kondo, S. Masaoka, Y. Pushkar, *J. Catal.* **2024**, *429*, 115230.

[118] a) K. G. Kottrup, D. G. H. Hetterscheid, *Chem. Commun.* **2016**, *52*, 2643–2646; b) D. G. H. Hetterscheid, *Chem. Commun.* **2017**, *53*, 10622–10631.

[119] K. G. Kottrup, S. D'Agostini, P. H. van Langevelde, M. A. Siegler, D. G. Hetterscheid, *ACS Catal.* **2018**, *8*, 1052–1061.

[120] S. Karim, A. Chakraborty, D. Samanta, E. Zangrando, T. Ghosh, D. Das, *Catal. Sci. Technol.* **2020**, *10*, 2830–2837.

[121] H.-T. Zhang, X.-J. Su, F. Xie, R.-Z. Liao, M.-T. Zhang, *Angew. Chem. Int. Ed.* **2021**, *60*, 12467–12474.

[122] H.-T. Zhang, Y.-H. Guo, Y. Xiao, H.-Y. Du, M.-T. Zhang, *Angew. Chem. Int. Ed.* **2023**, *62*, e202218859.

[123] Z.-K. Shen, K. Li, Z.-J. Li, Y.-J. Yuan, J. Guan, Z. Zoua, Z.-T. Yu, *Dalton Trans* **2024**, *53*, 17536–17546.

[124] a) A. Cingolani, D. Olivieri, A. Messori, C. Cesari, V. Zanotti, S. Zacchini, I. Gualandi, E. Scavetta F Mariani, D. Tonelli, R. Mazzoni, *Inorg. Chim. Acta* **2022**, *542*, 121138; b) A. Cingolani, C. Cesari, S. Zacchini, V. Zanotti, M. C. Cassani, R. Mazzoni, *Dalton Trans.* **2015**, *44*, 19063–19067; c) F. Calcagno, C. Cesari, A. Gagliardi, A. Messori, A. Piazzi, F. Tamassia, M. Garavelli, R. Mazzoni, I. Rivalta, *Cell Rep. Phys. Sci.* **2024**, *5*, 102291; d) C. Cesari, R. Mazzoni, E. Matteucci, A. Baschieri, L. Sambri, M. Mella, A. Tagliabue, F. Basile, C. Lucarelli, *Organometallics* **2019**, *38*, 1041–1051; e) C. Cesari,

A. Cingolani, C. Parise, S. Zacchini, V. Zanotti, M. C. Cassani, R. Mazzoni, *RSC Adv.* **2015**, *5*, 94707–94718.

[125] a) F. Arrigoni, L. Bertini, L. De Gioia, G. Zampella, R. Mazzoni, A. Cingolani, I. Gualandi, D. Tonelli V Zanotti, *Inorg Chim Acta* **2020**, *510*, 119745; b) F. Arrigoni, L. Bertini, L. De Gioia, A. Cingolani, R. Mazzoni, V. Zanotti, G. Zampella, *Inorg. Chem.* **2017**, *56*, 13852–13864; c) R. Mazzoni, A. Gabiccini, C. Cesari, V. Zanotti, I. Gualandi, D. Tonelli, *Organometallics* **2015**, *34*, 3228–3235.

[126] F. Moccia, L. Rigamonti, A. Messori, V. Zanotti, R. Mazzoni, *Molecules* **2021**, *26*, 2728.

[127] a) Z. Q. Wang, Z. C. Wang, S. Zhan, J. S. Ye, *Appl. Catal., A* **2015**, *490*, 128–132; b) S. M. Al-Zuraiji, D. Lukacs, M. Nemeth, K. Frey, T. Benko, L. Illés, J. S. Pap, *Reactions* **2020**, *1*, 16–36.

[128] M. M. Najafpour, R. Safdari, F. Ebrahimi, P. Rafighi, R. Bagheri, *Dalton Trans.* **2016**, *45*, 2618–2623.

Manuscript received: December 31, 2024
Revised manuscript received: March 6, 2025
Version of record online: April 24, 2025